6ICEGE
6th International Conference on Earthquake Geotechnical Engineering
1-4 November 2015
Christchurch, New Zealand

Liquefaction Research by Laboratory Tests versus In Situ Behavior

T. Kokusho[1]

ABSTRACT

Major advances in liquefaction research in the laboratory to understand the basic mechanisms in comparison with in situ behavior during previous earthquakes are reviewed. Then, several issues related to liquefaction triggering and post-liquefaction deformation are selected for further discussion in the author's perspective. These include effects of fines associated with aging, effects of gravels, effects of initial shear stress and lateral spreading and lateral flow due to void redistribution. It has been disclosed that a quite a few issues still remain to be settled in evaluating liquefaction onset and post-liquefaction deformations for improving engineering design, particularly for Performance-Based Design (PBD).

Introduction

A half century has passed since 1964 when two significant earthquakes occurred in the United States and Japan that triggered liquefaction research in geotechnical engineering internationally: the M9.2 Great Alaskan earthquake and the M7.5 Niigata earthquake. The earthquake damage in Niigata in particular was very peculiar, and drew considerable attention from the general public and engineering community. Namely, the failure modes of structures were different from those during past earthquakes in that structural failure due to seismic inertial loading was marginal in comparison to damage associated with liquefaction and loss in bearing capacity of the foundation ground. Immediately after these two earthquakes, basic research was conducted among international geotechnical groups involving laboratory studies to understand the liquefaction triggering mechanisms. These initial studies focused on clean sands as in Niigata, however subsequent studies included a variety of soils such as sands containing low-plasticity fines and gravels. Not only liquefaction triggering but also post-liquefaction deformation associated with cyclic mobility and flow-type failure were investigated in the laboratory tests. At the same time in situ liquefaction behavior during earthquakes was also investigated. It was really necessary to compare, calibrate and interpret lab test results in the light of actual soil behavior in situ, as there remained a number of items which could not be fully understood or explained in laboratory tests only.

In this paper, major developments in liquefaction research in this half century are briefly reviewed in terms of soil element tests in the laboratory and compared to in situ behavior observed from field studies. A few issues are then selected for further discussion in the author's own perspective. These include effects of fines associated with aging, effects of gravels, effects of initial shear stress and lateral spreading and lateral flow due to void redistribution. The discussions deal with not only liquefaction triggering mechanism but also post-liquefaction deformation evaluation, essential to performance-based design methods.

[1]Dr. Takaji Kokusho, Professor Emeritus, Chuo University, Tokyo, Japan, koktak@ad.email.ne.jp

Stress Conditions in Laboratory Tests versus In Situ

In order to understand the underlying mechanisms of liquefaction triggering following the Alaskan and Niigata earthquakes, a simplified soil element was first considered. The element was assumed to be subjected to K_0 stress conditions (with σ'_v the vertical effective stress and $\sigma'_h = K_0\sigma'_v$ the horizontal effective stress) and sheared by cyclic shear stress τ_d due to a vertically propagating seismic SH-wave in a level ground. This is illustrated in Figure 1 (a). This simplified stress condition, which still serves as a standard model for liquefaction potential evaluation in engineering practice, is normally reproduced in the laboratory by simple shear or triaxial tests as indicated in Figure 1 (b) or (c).

The first laboratory test to simulate seismic liquefaction in a soil element was performed by Seed & Lee (1966) using a triaxial apparatus. A saturated sand specimen was isotropically consolidated with an effective consolidation stress σ'_c, and the axial deviator stress σ_d was cyclically loaded in an undrained condition as in Figure 1 (c). This pioneering experiment demonstrated that the 100% pore-pressure buildup due to negative dilatancy (contraction when sheared) in cyclic loading is the key mechanism of seismic liquefaction.

The significant effect of effective confining stress on the liquefaction resistance was also noted during these experiments (Seed & Lee 1966). To account for this effect, the liquefaction resistance is normally expressed as the ratio of cyclic shear stress (for 100% pore-pressure buildup or the double amplitude (DA) axial strain amplitude ε_{DA}=5% in a given number of cycles) to the effective confining stress. This is called the cyclic resistance ratio (CRR). However, later studies discovered that CRR tends to decrease with increasing effective confining stress (Tatsuoka et al. 1981, Kokusho et al. 1983). In North American practice, this confining stress-dependency of CRR is considered in liquefaction potential evaluations by employing the overburden correction factor $K_\sigma = CRR_{\sigma'_c} / CRR_{\sigma'_{c=98kPa}}$ (Idriss & Boulanger 2008).

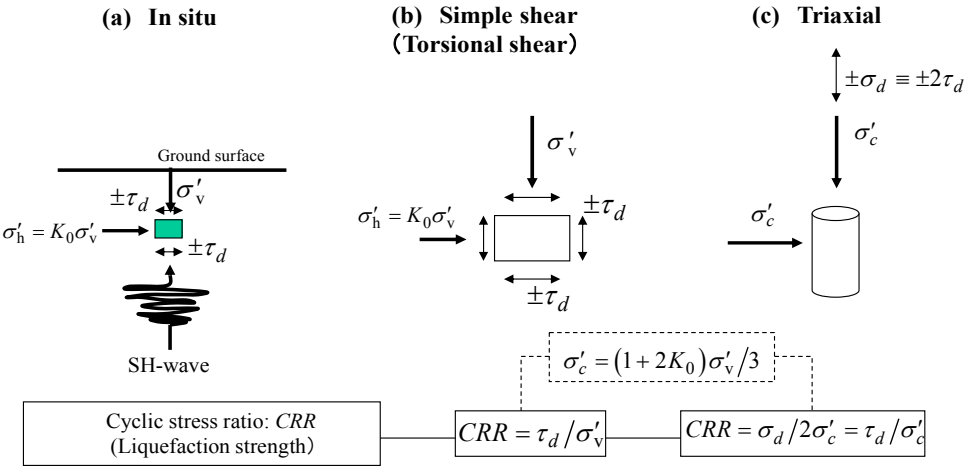

Figure 1. Comparison of stress conditions in situ and laboratory: (a) In situ, (b) Simple shear tests, (c) Triaxial tests and definitions of CRR.

Even today, the undrained cyclic triaxial test with isotropic consolidation and axial cyclic loading is a common laboratory test method for liquefaction evaluation, even though the stress state between the test specimen and in situ soils are quite different. The effect of the difference in stress condition was discussed by Seed & Peacock (1971) by comparing simple shear tests (b) and triaxial tests (c). A relationship was proposed $(\tau_d/\sigma_v')_{field} = c_r \times (\sigma_d/2\sigma_c')_{triax}$ to correct the triaxial test data to be representative of field conditions. The coefficient c_r relating the two stress ratios was determined to be in the range of 0.55~0.70 for clean sands with the relative density D_r =40~85%. Ishihara et al. (1977) conducted a similar experimental study using a hollow cylindrical torsional shear device that can reproduce a given K_0-consolidation for clean sand of D_r=55% with parametrically changing K_0=0.5, 1.0 and 1.5 keeping the vertical effective stress constant as σ_v' =98 kPa. Figure 2 (a) indicates that the cyclic stress ratio (CSR) defined by τ_d/σ_v' for 100% pore-pressure buildup ($\Delta u/\sigma_v'$ =1.0) is correlated with the number of cycles N_c differently for different K_0-values. However, if CSR is defined as τ_d/σ_c' as shown in Figure 2 (b), where $\sigma_c' = (1+2K_0)\sigma_v'/3$ is the effective confining stress, all the test results with different K_0-values are almost uniquely correlated with N_c. The above findings suggest that triaxial tests isotropically consolidated with $\sigma_c' = (1+2K_0)\sigma_v'/3$ may be almost equivalent to in situ soils in the K_0-condition. Some other studies do indicate that the CSR-value may not quite be uniquely determined by the effective confining stress σ_c' but deviated by a factor of 0.8~1.5 (Yamashita & Toki 1992).

As mentioned earlier, a simplified model of a K_0-consolidated soil element in a level ground sheared by seismic SH-wave is still serving as a standard model for liquefaction potential evaluation in the current engineering practice. However, most liquefaction-induced damage actually occurs near structures or slopes where the simplified stress system may not be applicable. In these situations, a more complex stress systems including sustained initial shear stress has to be considered. This significantly affects not only liquefaction triggering but also the post-liquefaction deformation mechanism. Laboratory test results considering the sustained initial shear stress compared to in situ liquefaction behavior will be discussed in a subsequent section.

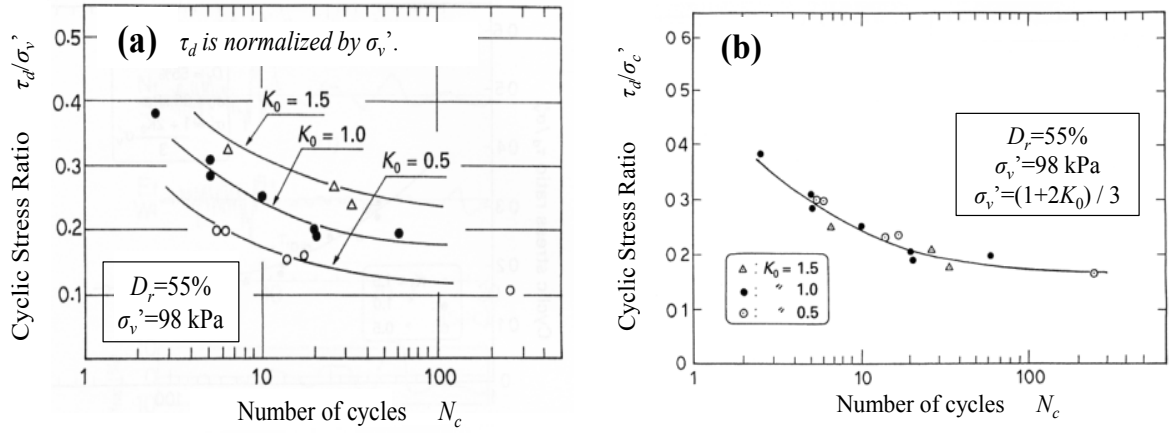

Figure 2. K_0-consolidated torsional simple shear test results for K_0=0.5, 1.0, 1.5: (a) Vertical axis normalized by σ_v', (b) Vertical axis normalized by σ_c'= (σ_v'+2σ_h')/3 (Ishihara et al. 1977).

Soil Density and Fabric in Laboratory Tests versus In Situ

From the early stages of liquefaction research, soil density was recognized as a key parameter controlling liquefaction susceptibility. Relative density D_r was used as a common scale for densities of non-cohesive granular soils because the absolute soil density is greatly influenced by particle grading. Several correlations were developed for clean sands between D_r and the cyclic resistance ratio based on laboratory tests on reconstituted sands. Figure 3 (a) shows a typical cyclic resistance ratio (CRR) versus D_r relationship for a clean sand obtained from undrained simple shear cyclic loading tests using a shake table (De Alba et al. 1976). The CRR tends to increase proportionally with increasing D_r up to a certain density, then increases dramatically depending on the single amplitude strain γ at which liquefaction is defined. If the onset of liquefaction is defined at larger strains, CRR increases significantly at lower values of D_r. Figure 3 (b) shows a similar result obtained by undrained cyclic torsional simple shear tests for clean Toyoura sand (Tatsuoka et al. 1982). It again indicates a linear CRR~ D_r relationship up to a certain D_r corresponding to the chosen value of double amplitude shear strain, followed by a sudden increase in the CRR.

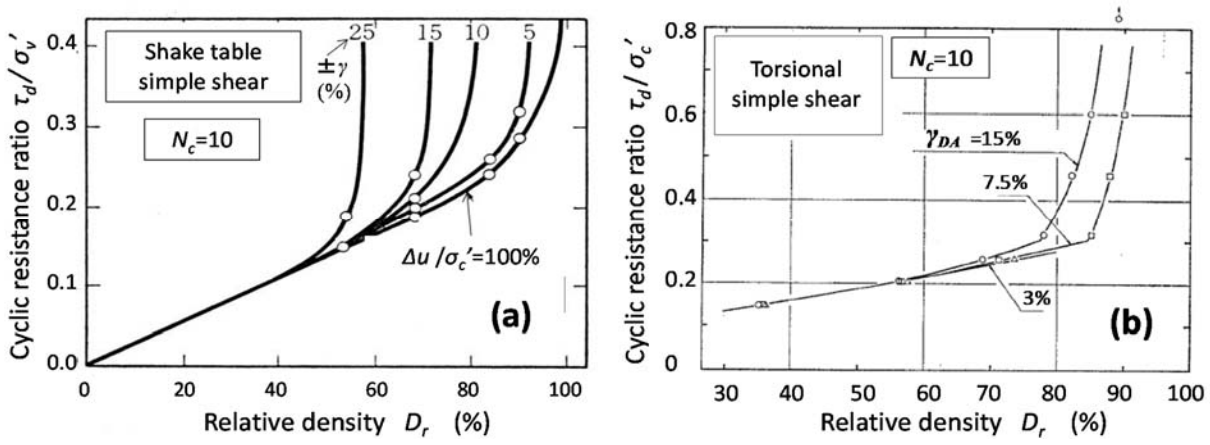

Figure 3. CRR corresponding to various strain amplitudes γ versus relative density D_r curves obtained from undrained simple shear tests for clean sands: (a) Shake table test results (de Alba et al. 1976), (b) Torsional simple shear test results (Tatsuoka et al. 1982).

Though it is quite clear that relative density D_r is one of the key parameters, the CRR-value is not uniquely determined solely by D_r. Figure 4 (a) shows CSR~N_c curves obtained by triaxial tests on clean sand specimens reconstituted by a variety of sample preparation methods (Mulilis et al. 1977). The curves are strikingly varied despite the same D_r=50% depending on different sample preparation methods used. The highest CRR is for samples prepared using high frequency vibration on moist samples and the lowest is for the air-pluviation (AP: dry sand is rained in air with a given fall height). This indicates that not only the relative density but also subtle changes in soil fabric introduced by different sample preparation methods make significant differences in CRR. Figure 4 (b) shows CRR versus D_r relationships obtained by torsional simple shear tests on reconstituted specimens by two sample preparation methods (Kokusho et al. 1983): Water Tapping (WT: sand deposited in water is tapped to densify) and AP. The difference in CRR between the

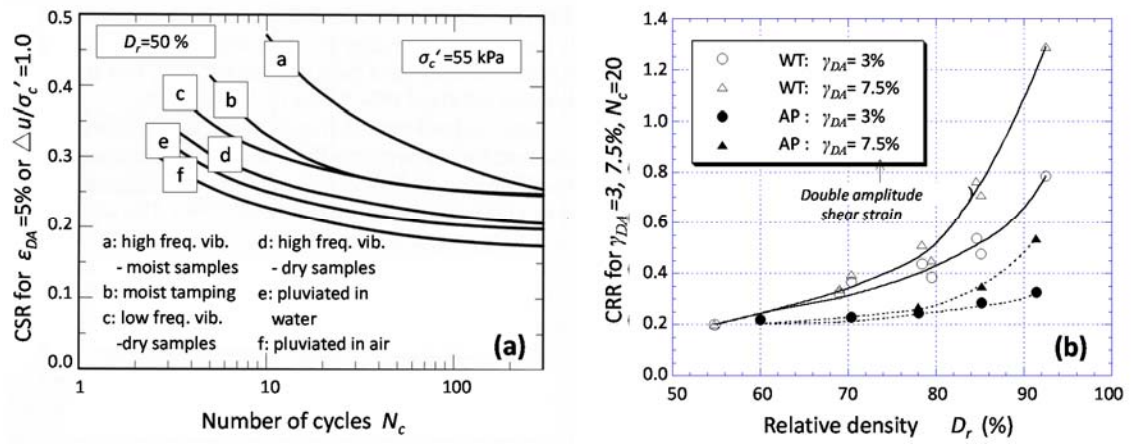

Figure 4. Effect of sample preparation methods on CRR of clean sands: (a) CSR~N_c curves of D_r =50% for sample preparations a~f (Mulilis et al. 1976), (b) CRR~D_r plots for WT & AP methods (Kokusho et al. 1983).

two sample preparation methods tends to grow with increasing D_r, presumably because the WT-method induces a stronger soil fabric to attain higher density than the AP-method. From the findings on reconstituted specimens, it may well be inferred that the CRR-value of natural sand deposits is not determined solely by the relative density but strongly influenced by in situ soil fabric that reflects the depositional, mechanical and geochemical histories of the soil.

Two typical long-term mechanical histories for in situ sands may be over-consolidation and pre-shearing effects. Over-consolidation, besides increasing the K_0-value and hence the effective confining stress σ_c', results in higher values of CRR even under the same σ_c' mainly due to a change in soil fabric. Although the observed effect varies somewhat among researchers depending on the differences in sands tested and test methods (Ishihara & Takatsu 1979, Kokusho et al. 1983, Tatsuoka et al. 1988), it may be approximated by the simple formula $CRR/CRR_{OCR=1} = (OCR)^m$,

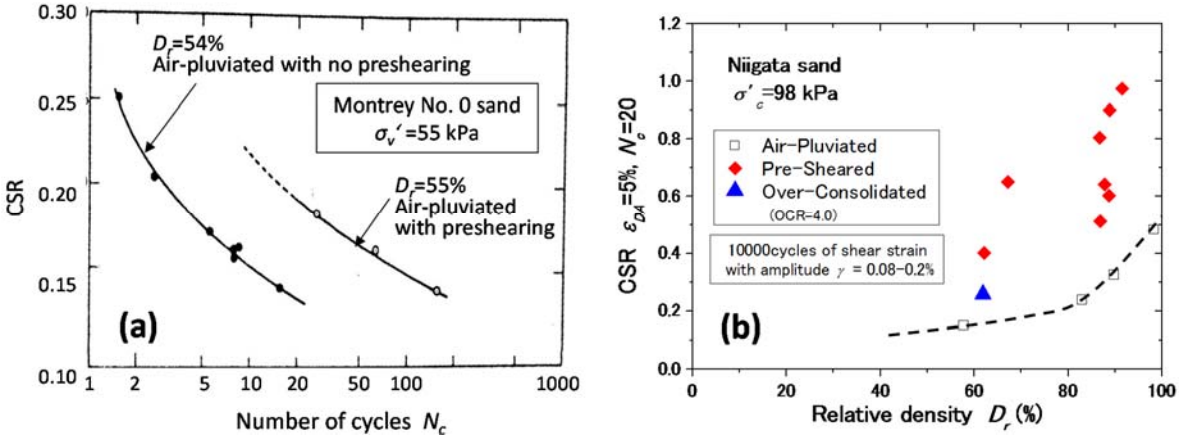

Figure 5. Effect of small-strain preshearing on AP clean sands: (a) CSR~N_c curves with/without preshearing by shake-table simple shear tests (Seed et al. 1977) and (b) CRR~D_r plots with/without preshearing and with over-consolidation by cyclic triaxial tests (Tokimatsu et al. 1986).

where the power m varies m=0.1~0.5. Another suspected long-term effect in situ is the low-strain pre-shearing due to a number of small seismic vibrations that soils may experience after deposition. Figure 5 (a) compares CSR~N_c curves obtained by a simple shear test using a shake table for the same clean sand prepared by the AP method, without or with the addition of a given number of low-strain preshearing representing several small seismic shocks (Seed et al. 1977). The latter shows higher liquefaction resistance by about 50% than the former even though the D_r is almost identical. The effect of preshearing was also investigated by Tokimatsu et al. (1986) in triaxial tests in which ten thousands cycles of 0.08~0.2% axial strain were applied to dense AP sand specimens. Figure 5 (b) indicates a surprisingly large effect of the preshearing, doubling or tripling the CRR-values of AP-sands with a minimal change in D_r. The preshearing effect observed here is much more dominant than the overconsolidation effect of OCR=4.0, which is also plotted in the same figure.

How to Determine In Situ CRR for Liquefaction Triggering

The results of previous research indicated that liquefaction resistance cannot be determined solely by the relative density. It is very much influenced by how in situ soils were deposited and what kind of stress/strain histories they experienced since then. This implies that laboratory liquefaction tests if possible have to be done on intact samples which are recovered in situ. It is however, difficult to sample sandy soils and still preserve not only in situ densities but also in situ fabric. Sand samples tend to be disturbed very easily due to small vibrations and shocks during sampling and laboratory handling.

Figure 6 (a) demonstrates by a simple laboratory test how significantly vibrations and shocks may affect soil fabric and liquefaction resistance (Kokusho et al. 1986). Triaxial test specimens of clean Toyoura sand were prepared with relative densities D_r≒70~95% by the WT method to induce a strong fabric. Then, the dewatering specimen was put on the brass cup of a liquid-limit test device and given a certain number of small (1.25 mm height) drops N_{drop} to mimic vibrations and shocks possibly imposed during sampling and laboratory handling. The CRR-values for ε_{DA}=5%

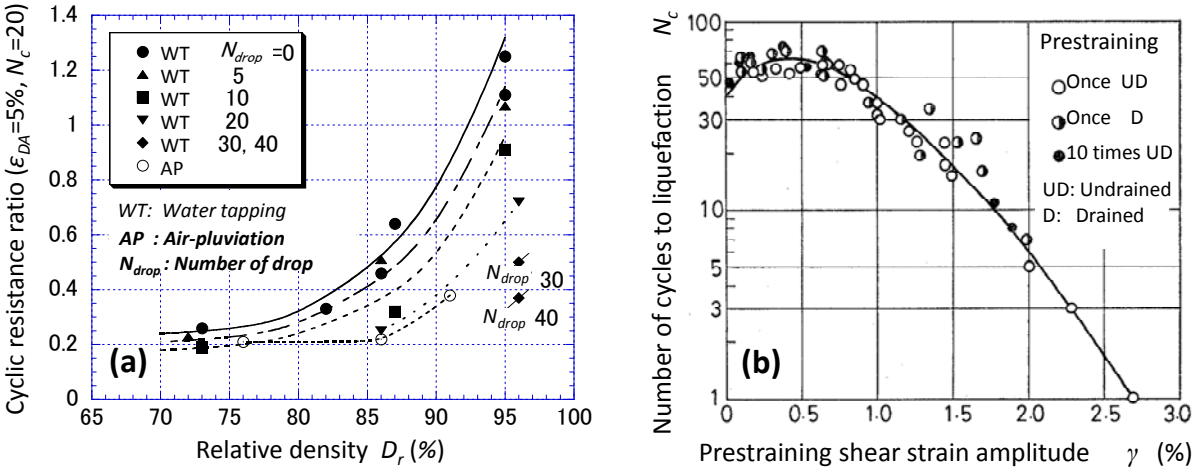

Figure 6. Effect of disturbance on liquefaction resistance: (a) Effect of dropping dewatered test specimens 1.25 mm a given number of times N_{drop} (Kokusho et al. 1985),
(b) Prestraining effect by various amplitude shear strains (Suzuki & Toki 1984).

in N_c=20 clearly decreased with increasing N_{drop} for higher D_r in particular (down to 1/4 of CRR for N_{drop} =0 in the extreme) and almost coincide with those of the specimens prepared by the AP method. The test results vividly show that soil fabric induced by the WT method is very easy to deteriorate by a series of faint shocks, even though D_r does not change significantly. Unlike the internal friction angle of sand, which is almost uniquely determined by D_r, liquefaction resistance is very much dependent on microscopic soil fabric which is not easy to preserve in the normal sampling practice. In Figure 6 (b), a variable preshearing strain amplitude γ is given with a different number of cycles to triaxial clean sand specimens to see its effect on the number of cyclic loading N_c for the onset of liquefaction in subsequent undrained cyclic loading tests (Suzuki & Toki 1984). The test results clearly indicate that prestraining history will considerably reduce the liquefaction resistance if the strain is larger than $\gamma \fallingdotseq 1\%$, though it tends to increase the resistance for strains smaller than this. Thus, great care is needed to avoid straining exceeding a threshold during sampling and handling of in situ sands.

The best way to directly evaluate in situ CRR-values in laboratory tests would be to obtain intact samples by in situ freezing and drilling or block sampling by hand very carefully. For in situ freezing, sands are first frozen by circulating a coolant through underground vertical tubes. The frozen sands are then cored to recover intact samples, cut and trimmed for laboratory tests, set up in test devices under in situ stresses, and then tested after thawing (Yoshimi et al. 1978). This technique is generally believed to have very little impact on soil fabric, however it is very costly. Yoshimi et al. (1994) demonstrated that this sampling method yields CRR-values from triaxial tests that are markedly higher for sands with $D_r \geq 60\%$ than those of conventional tube sampling. In contrast, soils obtained by conventional sampling methods show very little D_r–dependent increase in CRR-values up to D_r=80%, presumably due to the effects of disturbance during sampling. In the case of block sampling which is carried out in dewatered trenches, unsaturated soil samples

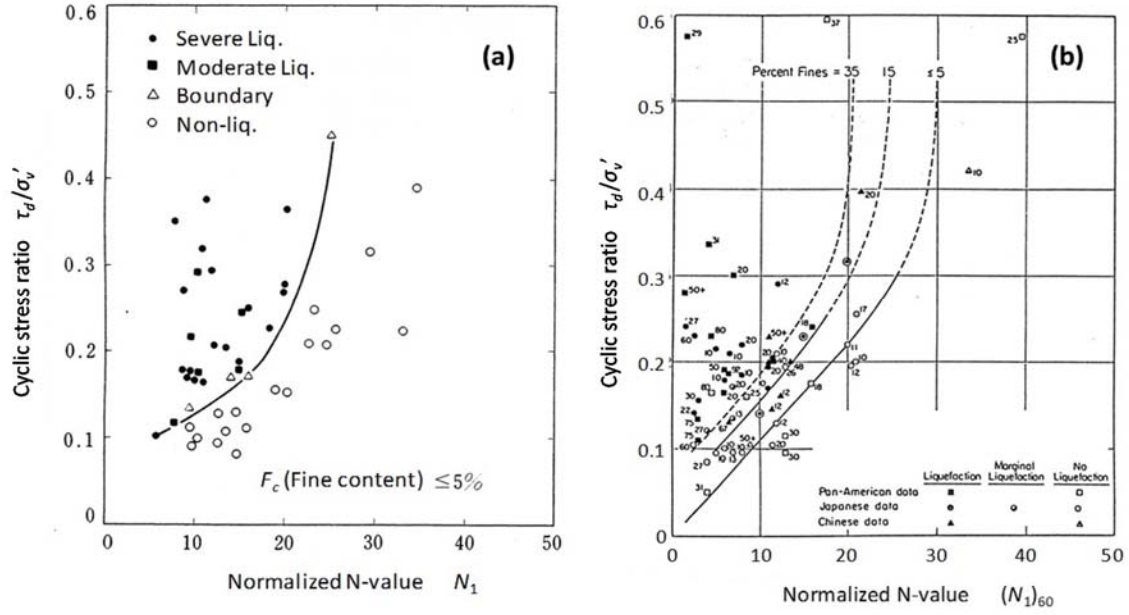

Figure 7 CSR correlated with SPT resistance, drawing a boundary curves (CRR) based on liquefaction case histories: (a) Tokimatsu & Yoshimi (1983), (b) Seed & De Alba (1984).

are carved out and stored in metal or plastic tubes that are carefully pushed down around the soil. This sampling procedure may not be completely immune from disturbance effects.

In normal engineering practice, where undisturbed sampling plus laboratory tests are too costly, CRR is determined by in situ tests such as Standard Penetration Tests or Cone Penetration Tests. The penetration resistance of SPT or CPT is recognized to have a close correlation with relative density. However, it is quite doubtful whether the effect of subtle soil fabric is reflected in the results of these penetration tests because the penetration process is quite destructive.

The penetration resistance versus CRR correlation was first developed empirically using liquefaction case histories from previous earthquakes (Tokimatsu & Yoshimi 1983, Seed & De Alba 1984). Cyclic stress ratios at many sandy soil sites estimated from site-specific PGAs (based on earthquake magnitudes, hypocentral distances and soil conditions) were plotted versus associated penetration resistances, and a boundary curve most properly segregating liquefied and non-liquefied plots was identified as the CRR versus penetration resistance curve for liquefaction potential evaluations as shown in Figure 7. Liquefaction/non-liquefaction at each site in case histories was judged by liquefaction manifestations at the ground surface such as sand boils, cracks, surface settlements and structural settlements. This method, employed as the North-American practice in evaluating liquefaction potential (Idriss & Boulanger 2008), appears to be quite demonstrative because it is based on the actual field performance. However, because it largely depends on evidence at the ground surface, the reliability tends to decrease with increasing soil depth. In this regard, research efforts continue in order to improve its reliability on the surface manifestations depending on liquefaction depth (e.g. Maurer et al. 2015).

In Japan, the penetration resistance versus CRR correlation was developed mainly by combining undrained cyclic triaxial tests on intact soils sampled by situ freezing from various sand deposits and associated penetration tests in the same deposits (Yoshimi et al. 1994, Suzuki et al. 1995,

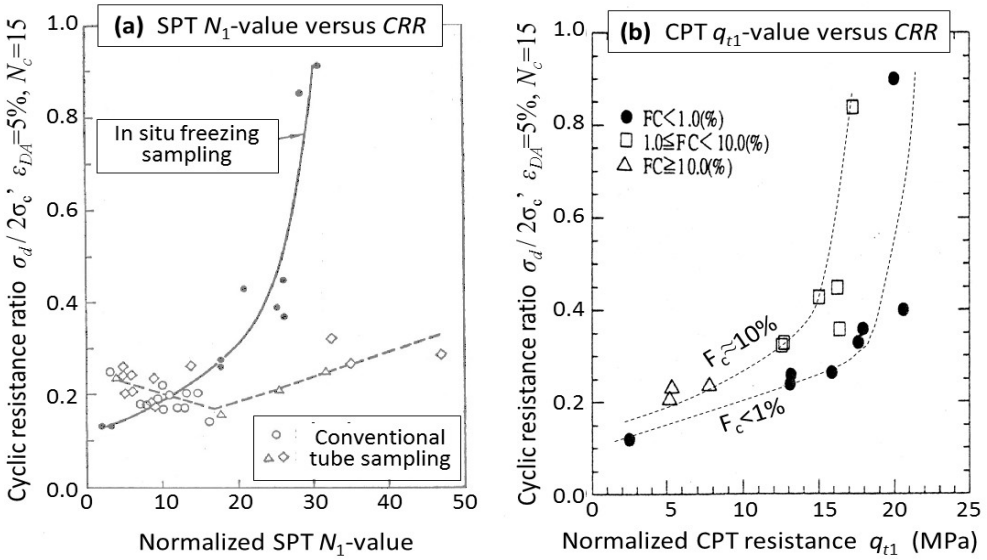

Figure 8. CRR determined by triaxial tests on intact samples by in situ freezing versus penetration resistances: (a) SPT (Yoshimi et al. 1994), (b) CPT (Suzuki et al. 1995).

Matsuo 1997). As already mentioned, this sophisticated sampling technique yields distinctively higher CRR-values for dense sands with high penetration resistances when compared with conventional tube sampling methods as plotted in Figure 8 (a) (Yoshimi et al. 1994). A similar relationship of CRR-values versus normalized CPT resistances q_{t1} is shown in Figure 8 (b), which also shows a clear increase in CRR with increasing q_{t1} (Suzuki et al. 1995). Unlike the field-based correlations previously mentioned, the laboratory test-based correlations are not directly demonstrated by in situ performance; however the liquefaction resistance can be determined by the same standard to great depths.

The compatibility of the above mentioned laboratory test-based and field-based approaches has been recognized in Figure 7 (a) where the curve segregating liquefied/non-liquefied plots successfully is actually based on the solid curve in Figure 8 (a) assuming K_0=0.5. Another study was conducted to compare the two approaches using the same database from the same sites, and the results indicated that under particular conditions specified in the design code (Japan Road Association 2012), they were compatible with each other (Matsuo 1997).

Effect of Fines and Aging

From liquefaction case histories after the 1964 Niigata earthquake, it was increasingly recognized that sands containing non/low-plastic fines are as liquefiable as clean sands. Figure 9 (a) shows the triangular classification chart of liquefied sand during earthquakes worldwide before 1980 summarized by Tokimatsu & Yoshimi (1983). It indicates that, while soils with fines content F_c as high as 60-70% have liquefied, none of the soils with clay contents C_c > 20% liquefied. This is in good agreement with a study from China (Seed and Idriss 1981). According to another study in China (Finn 1982), a plasticity index I_p=10 seems to be a threshold for liquefaction. Figure 9 (b) summarizes physical properties of sand boils erupted from reclaimed soils during 4 earthquakes (Mori et al. 1991), indicating that erupted sands have clay contents mostly C_c<10% despite very high fines content $F_c \fallingdotseq 100\%$. All these case histories indicated that fines-containing sands are as liquefiable as clean sands if the fines are low/non-plastic.

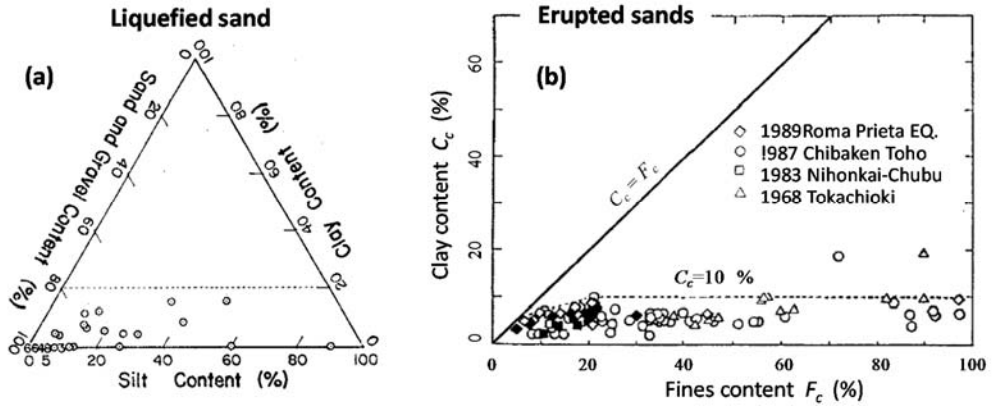

Figure 9. Physical properties of sands containing fines liquefied in previous earthquakes:
(a) Triangular classification of liquefied sands (Tokimatsu & Yoshimi 1983),
(b) F_c versus C_c plots for erupted sands (Mori et al.1991).

Figures 10 (a), (b), (c) show the results of a systematic cyclic triaxial test program using soil specimens containing a variety of fine soils (I_p =0~51, F_c=10~67%, C_c=9~28%) to see how their properties influence CRR-values (Koseki et al. 1986). Obviously, the physical properties have definite effects on CRR, among which plasticity index I_p and clay content C_c show a clear positive correlation with CRR. This indicates that these two variables, representing the cohesion of fines, can serve as relevant indices for screening liquefaction potential. In contrast, F_c is not so closely correlated with CRR, probably because F_c does not directly represent soil plasticity as I_p or C_c do.

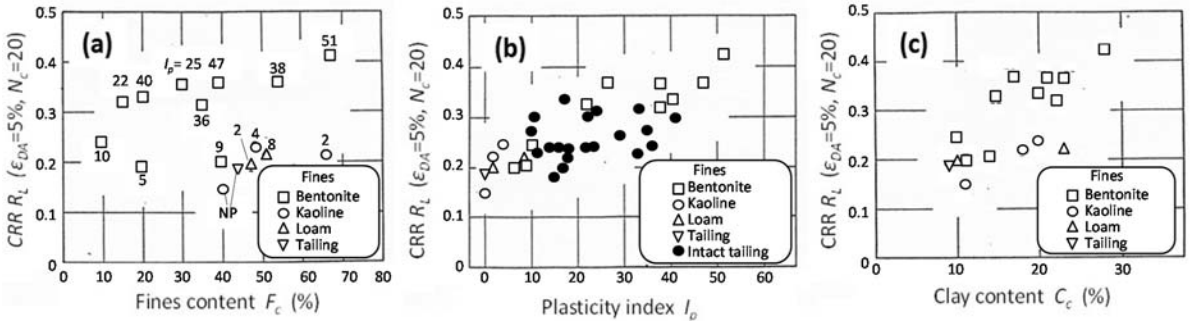

Figure 10. Effects of fines content F_c (a) , plasticity index I_p (b), clay content C_c (c), on CRR of fines-containing sands from cyclic triaxial tests (Koseki et al. 1986).

During the 2011 Tohoku earthquake in Japan (M9.0), liquefaction occurred extensively along the Tokyo bay area, which was more than 200 km from the nearest edge of the earthquake fault. In Urayasu city in particular, shown in Figure 11 (a), extensive liquefaction occurred in a wide area with groundwater tables -1.0 to -2.0 m deep, newly reclaimed after 1968 by hydraulically filling of sea-bed soils. A huge amount of ejecta containing lots of fines, which were all non-plastic, covered the ground surface and there was at least 0.1~0.3 m subsidence. In contrast, another area of the same city that existed before 1948 did not liquefy, despite very similar soil profiles and soil properties. There are many bore-holes and SPT loggings available in this area as depicted in Figure 11 (a). These indicate similar soil profiles all over Urayasu consisting of surface land fill (B-layer), an alluvial sand layer (As-layer) and underlying Holocene soft clay. The clay layer was 30 to 40 m thick underlain by Pleistocene dense sand with N>50. A significant difference in the soil profiles was the existence of hydraulic fill (F-layer) between the B and As-layers in the reclaimed areas, while it was missing in the non-reclaimed area. Hence, it is generally believed that the F-layer was responsible for the liquefaction during the earthquake. Figure 11 (b) shows variations of clay content C_c with depth at 11 boreholes in the liquefied area, where soil profiles are composed of the B-layer, F-layer and As-layer from the ground surface to 16 m deep. The plots are connected with either thick solid lines in the F-layer or thin dotted lines in the B and As-layers. The soils are very variable along the depth, with interbedded sublayers of high C_c or I_p that appear very unlikely to liquefy. Nevertheless, widespread non-plastic ejecta covered the ground surface, and the subsidence strain in the liquefied deposits exceeded 5% at many points as will be seen in Figure 12. This possibly suggests that intensive liquefaction occurred exclusively in soils with small C_c, overwhelming the soils with higher C_c or I_p. This indicates that sand deposits containing fines of higher plasticity than normally classified as liquefiable, may not be free from liquefaction if they are interbedded by liquefiable sands containing non/low-plastic fines, and may possibly erupt considerable non-plastic ejecta to the ground surface as in Urayasu. The previous experiences with nonplastic ejecta in reclaimed deposits shown in Figure 9 (b) also suggest this possibility.

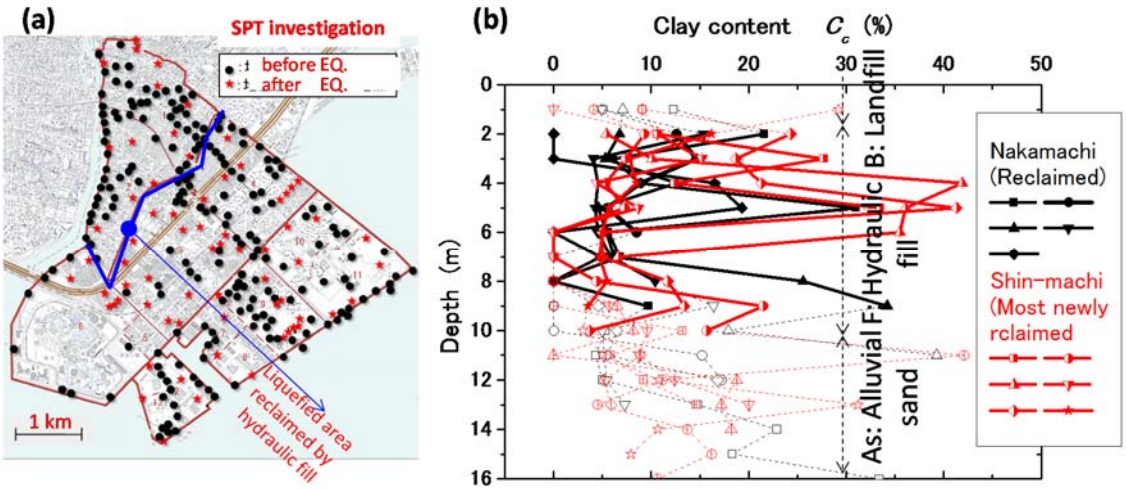

Figure 11. Urayasu city map with locations of soil investigation boreholes (a) and variations of clay content C_c along depth at different boreholes in reclaimed area (b) (Kokusho et al. 2014).

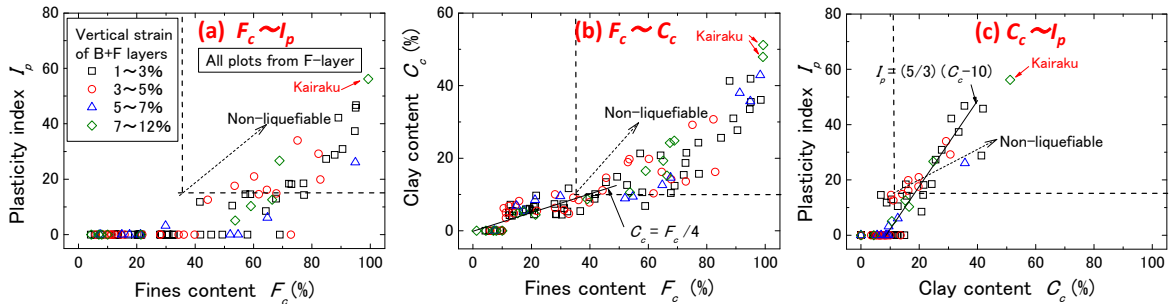

Figure 12. Cross-correlations between physical properties of liquefied hydraulically-filled layer in Urayasu with stepwise subsidence strains: (a) F_c~I_p, (b) F_c~C_c, (c) C_c~I_p (Kokusho et al. 2014).

In Figures 12 (a), (b), (c), correlations between F_c~ I_p, F_c~ C_c and C_c~ I_p are shown, respectively. All these properties were obtained from soils in the liquefied F-layer sampled after the earthquake in Urayasu by the SPT split spoon. The properties are widely varied; F_c=0~100%, I_p =0~60 and C_c=0~50%, indicating that soils experiencing widespread liquefaction were very variable in plasticity. This finding is in a good agreement with that already reported by Yoshimi (1991) for the same reclaimed land before the earthquake. Clear correlations are visible between the properties, among which approximation lines $C_c = F_c/4$ for $F_c \le 50\%$ and $I_p = (5/3)(C_c - 10)$ for $10 \le C_c \le 40$ are superposed in the charts. In each chart, horizontal and vertical dashed boundary lines are drawn corresponding to Japanese criteria (e.g. Specifications for Highway Bridges 1996) with which soils are initially screened for liquefaction susceptibility; $F_c \le 35\%$, $I_p \le 15$ and $C_c \le 10\%$. The plots in the charts are classified into four groups depending on earthquake-induced subsidence strains, which were calculated from the ground surface subsidence divided by the total thickness of F plus B layers, because the F-layer is considered to have liquefied by itself and presumably the B-layer liquefied by upward seepage flow. Despite the difficulty in interpreting

the data (because only a single strain value can be determined at each soil investigation site, while SPT-based physical properties have multiple values at individual depths of the same site), it may be said that the locations for larger subsidence strains (more extensive liquefaction) tend to be in zones of smaller I_p and smaller C_c, with the exception of some abnormal data belonging to a specific site (Kairaku). In contrast, a larger number of locations with larger strains are associated with larger F_c, indicating that F_c may not be a better index than I_p and C_c for screening liquefiability.

In engineering practice, the liquefaction potential of soils, initially screened by the criteria in terms of index properties, is then evaluated using SPT or CPT penetration resistances as already mentioned. If sands contain a measurable amount of low/non-plastic fines, the boundary curve between liquefaction and non-liquefaction is modified so that the liquefaction strength is raised for the same penetration resistance in accordance with the fines content F_c. The modification seems to be necessary because the penetration resistance cannot uniquely predict CRR by itself, necessitating another parameter such as fines content. This F_c-dependent modification of liquefaction strength originated from liquefaction case studies (Tokimatsu and Yoshimi 1983, Seed and De Alba 1984), in which empirical boundary curves separating liquefaction from non-liquefaction behavior, were found to be strongly dependent on fines content as observed in Figure 7 (b). The same F_c-dependency was also observed from laboratory cyclic loading tests on intact samples as shown in Figure 8 (b) (Suzuki et al. 1995). In contrast to these findings, however, a number of laboratory studies involving reconstituted specimens prepared to the same relative density (Kokusho 2007) or void ratio (Papadopoulou and Tika 2008), have shown that CRR clearly decreases with increasing F_c for low plasticity fines from F_c=0% to 30%. Thus, there is still a lack of understanding in relation to the effects of fines on both cyclic resistance and penetration resistance for the evaluation of liquefaction potential.

In order to clarify the basic effects of fines on the relationships between CRR and penetration resistance, a systematic experimental study was undertaken in which miniature cone penetration and subsequent cyclic loading tests were performed on triaxial test specimens under isotropic effective confining stress σ_c'=98 kPa (Kokusho et al. 2012). The results of the two tests on the same specimen were compared to develop direct q_t – CRR correlations for sands containing various amounts of non-plastic fines. In Figure 13 (a), the CRR-values for ε_{DA}=5% in N_c=20 are plotted

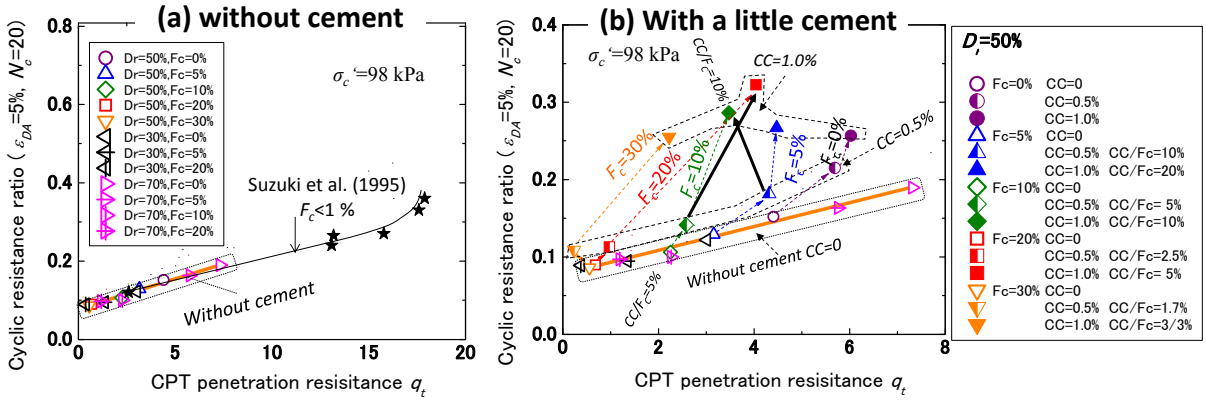

Figure 13. CRR-values plotted versus penetration resistance in triaxial test specimens by miniature cone penetration and subsequent cyclic loading tests: (a) Without cement, (b) With cement (Kokusho et al. 2012).

versus the mini-cone resistances q_t in the horizontal axis. The open symbols in the figure are located along a thick straight line in the chart despite wide variation in D_r (30~70%) and F_c (0~30%), indicating that the liquefaction strength is uniquely correlated to q_t irrespective of differences in D_r and F_c. This finding is quite contradictory with the current practice of liquefaction potential evaluation, where CRR is increases with increasing F_c. This finding may point to a significant difference between unaged reconstituted specimens in the laboratory and aged soils in situ. It should be noted that the star symbols in the diagram, by the way, are based on in situ CPT and associated triaxial tests on intact clean sands sampled by in situ freezing (Suzuki et al. 1995). The results from these two different studies coincide surprisingly well.

In order to investigate the aging effect, a small quantity of cement was added to fines-containing sand to simulate cementation or geochemical bonding in a short-term (curing time 24 hours) accelerated test**.** Penetration resistance q_t and CRR were measured in the same specimens to investigate the aging effect on the q_t - CRR correlations considering the fines content as a key parameter. Half-closed and closed symbols in Figure 13 (b) are from the accelerated tests on specimens with the cement content $CC \leq 1\%$. For example, the plots of a given F_c move up as indicated by the dashed arrows in the diagram from open (CC =0) to half-closed (CC =0.5%) to full-closed symbols (CC =1.0%). Obviously, the cementation tends to increase CRR more than q_t, so that the new plots move higher than the CC=0 line, indicating that CRR in liquefaction tests is more sensitive to the delicate change in fabric than q_t in destructive penetration tests. A parameter CC/F_c changing here from 0 to 20% with increasing CC may be considered to reflect a geochemical activity of fines. Specimens with higher CC/F_c may be considered older in geological age because of a stronger cementation effect. This indicates that, for the same CC/F_c –value (simulating the same cementation effect) exemplified by thick arrows for CC / F_c =5% or 10% in the Figure 13 (b), higher F_c-values result in higher liquefaction resistance for the same cone resistance. This trend is compatible with the liquefaction potential evaluation practice currently employed. Thus, the mini-cone plus cyclic triaxial tests utilizing a small amount of cement indicates that not the fines content itself but the cementation by geochemical aging is responsible for higher liquefaction strength for larger F_c under the same cone resistance, and this provides the basis of F_c-dependent modification of CRR in the liquefaction evaluation practice.

In the present liquefaction evaluation approaches using penetration resistance, the aging effect in terms of hundreds or thousands years cannot be determined because the penetration process is too destructive to discern delicate soil fabric developed during aging. Measurement of shear-wave velocity (V_s) has been considered to be a promising in situ test that may be able to differentiate subtle changes in soil fabric affecting CRR because of its non-destructive nature, and the database is increasing for that purpose (Andrus & Stokoe 2000). However, it should be pointed out that the V_s versus CRR relationship is not unique but soil-dependent (Sasaoka & Kokusho 2015). Hence, the combination of penetration tests and Vs-measurements seems to be promising to quantify the aging effect on CRR in in situ tests.

Effect of Gravels

Since the 1964 Niigata earthquake, liquefaction research on granular soils has been focused mainly on poorly-graded sandy soils. However, liquefaction of gravelly soils, though less frequent, has increasingly been witnessed during recent earthquakes. During the 1983 Borah Peak earthquake

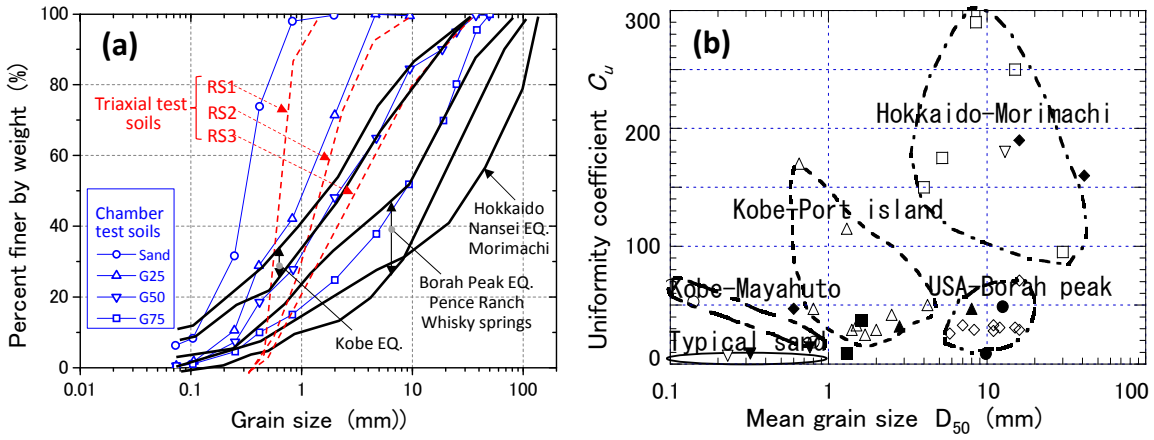

Figure 14. Grain size characteristics of gravelly soils: (a) Grain size curves of liquefied soils and soils tested in triaxial and calibration chamber tests, (b) Mean grain size D_{50} versus uniformity coefficient C_u plots of liquefied soils.

in Idaho, USA, fluvial sandy gravel deposits liquefied extensively triggering sand boils, ground fissures and lateral spreads (Andrus 1994). The N-value of the loosely deposited sandy gravel layers was 5-9 and values of shear-wave velocity ranged from 90-160 m/s. During the 1995 Hogoken Nambu earthquake in Japan, man-made deposits in Kobe reclaimed by decomposed granite soils containing large quantities of gravel and fines liquefied extensively. The SPT N-values were as low as 5 to 15 (e.g. Inagaki et al. 1996). During the 1993 Hokkaido Nansei-Oki earthquake, rock debris avalanche soil containing large size rocks as well as sands and silts liquefied in Mori town in Hokkaido, Japan, causing differential settlements of wooden houses. SPT N-values were 8 to 16 and values of shear-wave velocity in shallow depths were unbelievably as low as 60-90 m/s (Kokusho et al. 1995). Besides these cases, liquefaction of gravelly soils was also reported during the 1948 Fukui earthquake in Japan, the 1964 Alaskan earthquake, and others.

Figure 14 (a) exemplifies typical grain size distributions of the gravelly soils that liquefied recently with solid curves. They are all well-graded and actually a mixture of gravels, sands and even finer soils. In Figure 14 (b), the mean grain size (D_{50}) is plotted versus the uniformity coefficient (C_u= D_{60}/D_{10}) for the same gravelly soils. So far, the upper limits for D_{50} and C_u are about 20 mm and 300, respectively, but no limit may be reasonably justified. This indicates that gravelly soils, if their relative densities are low enough, can liquefy no matter how well-graded and how coarse they may be. Absolute dry densities of these well-graded gravelly soils are much higher than typically poorly-graded sands. However, gravelly soils are sometimes deposited very loosely with low values of relative density, exhibiting very low N-values and shear-wave velocities as already mentioned. In sandy-gravels, one may imagine that only sandy soils are responsible for liquefaction, while gravel particles are only floating in the sandy portion. This view may be justified in gap-graded gravelly sands where the sandy fraction is so large that there is no direct contact between gravel particles. This seems unlikely in the well-graded soils shown in Figure 14 (a), where large gravel particles were considered to take part in liquefaction. Also note that the permeability of natural well-graded gravelly soils may not be high enough to retard the pore-pressure buildup, because particles of sands and fines filling the voids of gravels tend to make the permeability no higher than sandy soils, 10^{-2}~10^{-3} cm/s.

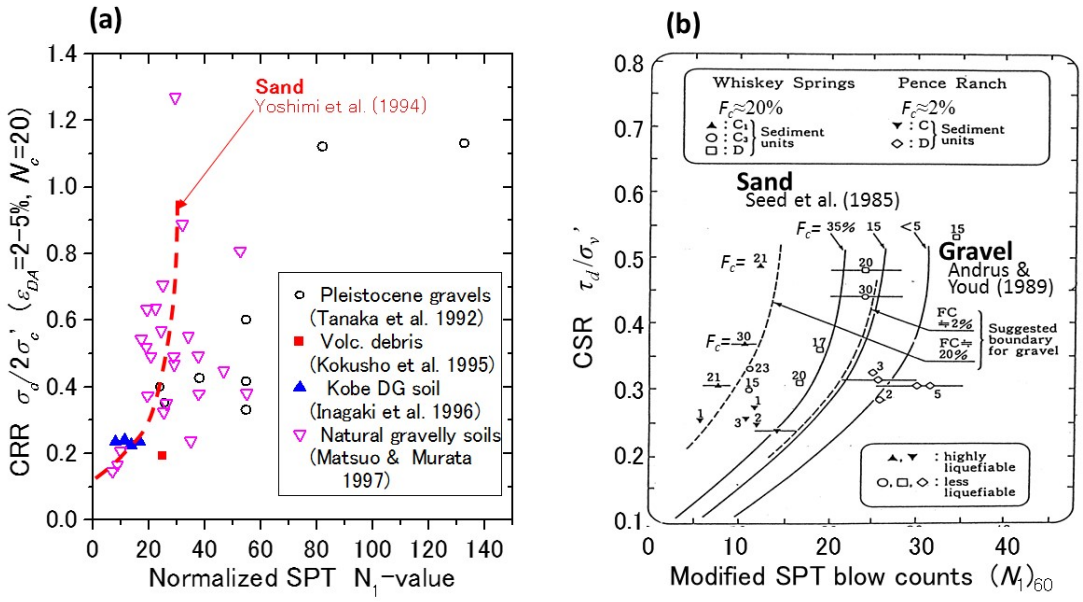

Figure 15. CSR or CRR versus SPT blow counts for gravelly soils obtained by two different approaches: (a) Triaxial tests on intact samples (Tanaka et al. 1992, Kokusho et al. 1995, Inagaki et al. 1996, Matsuo & Murata 1997), (b) Case study during the Borah Peak earthquake (Original data by Andrus & Youd 1985, modified by Ishihara et al. 1992).

Figure 15 (a) summarizes undrained cyclic triaxial test results of intact gravelly soils in terms of CRR versus SPT N_1 plots (Tanaka et al. 1992, Kokusho et al. 1995, Inagaki et al. 1996, Matsuo & Murata 1997). All the samples here were recovered by in situ freezing sampling and tested under isotropic confining stress. The CRR-values, $\sigma_d/2\sigma_c'$, defined as the stress ratio for 2-2.5% or 5% double amplitude strain in the number of cycles N_c=15 or 20, for gravels are largely scattered and mostly lower than those for sands of the dashed curve by Yoshimi et al. (1994) for N_1 ≥20-25 in particular.

Figure 15 (b) shows boundary curves for liquefaction (CSR=τ_d/σ_v', versus modified SPT N-value, $(N_1)_{60}$) obtained by Andrus and Youd (1989) based on the case study of gravelly soils during the 1983 Borah Peak earthquake. These curves separating liquefaction/non-liquefaction plots were based on the manifestation of sand boils, fissures and lateral spreading. Compared with the similar curves for sand (dashed curves) proposed by Seed et al. (1985), the CRR-value of gravels seems to be higher than sand (Ishihara et al. 1992). This trend contrasts with that shown in Figure 15 (a), where gravelly soils exhibit lower liquefaction resistance than sandy soils of the same N_1-value in the laboratory tests on intact gravelly soils.

In order to understand these differences in the liquefaction resistance of gravelly soils, three granular soils with different particle gradations were compared in undrained cyclic triaxial tests (Kokusho et al. 2004). The soils RS1, RS2 and RS3 (C_u=1.44, 3.79 and 13.1) shown in Figure 14 (a) were reconstituted from fluvial sands and gravels, with sub-round hard particles. The specimens were 100 mm in diameter (about 5 times the maximum particle size for RS3) and 200 mm in height, prepared to a wide range of relative densities D_r≒10%~100%, and were isotropically consolidated

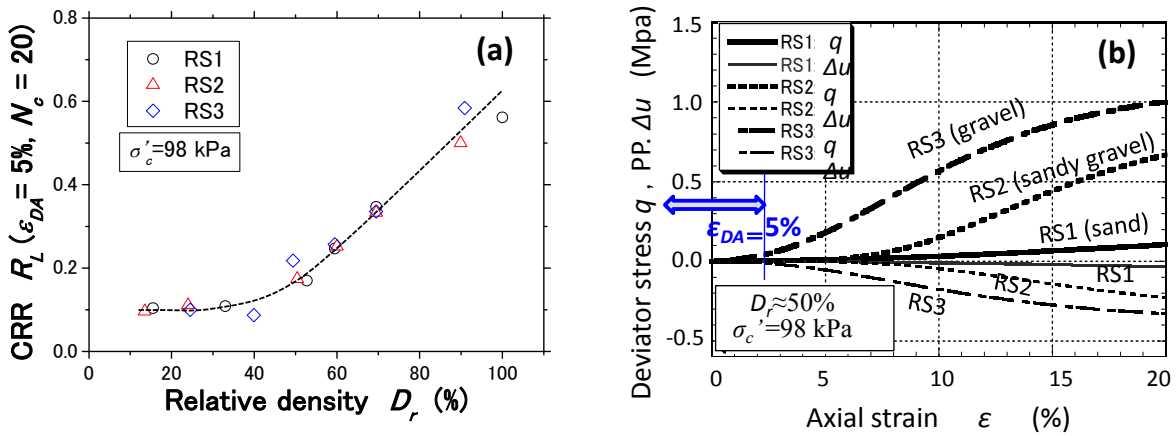

Figure 16. Comparison on 3 granular soils (RS1, RS2, RS3) with different particle grading: (a) CRR versus D_r plots by cyclic loading tests (Kokusho et al. 2004), (b) Deviatoric stress q versus axial strain ε by post liquefaction monotonic loading tests (Kokusho 2007).

to σ_c'=98 kPa. In Figure 16 (a), the CRR-values for ε_{DA} =5% for N_L =20 are plotted versus relative densities D_r. The data points for soils RS1, RS2 and RS3 are apparently aligned along a unique curve although there is some scatter for D_r≒50% and 90%. It may be said that CRR defined by attaining double amplitude strain ε_{DA}=5% is strongly dependent on D_r despite large differences among the three soils in absolute densities due to the differences in particle gradation or uniformity coefficient C_u. In other words, liquefaction strength or CRR (normally defined corresponding to ε_{DA}=5%) is dependent not so much on the particle gradation but very much on the relative density.

Regarding the above test results, the relationship between relative density D_r and SPT-N_1 values had been investigated for sandy and gravelly soils in another test program employing a large calibration chamber shown in Figure 17 (a) by Kokusho & Yoshida (1997). The standard penetration tests were carried out in four granular soils with parametrically changing uniformity coefficients, C_u=1.95 to 31.1 (sand, G25, G50, G75 with grain size curves also shown in Figure 14 (a)) in the K_0-consolidation with overburden stresses σ_v'=49~686 kPa applied by a rubber bag beneath the chamber cap. Figure17 (b) shows the normalized SPT N-value versus D_r relationships, obtained for the 4 soils. These are approximated by an empirical formula written in the chart (Kokusho 2007). This indicates that well-graded gravel (G75) shows a larger increase in the N-value with increasing D_r than poorly-graded sand (TS), and the difference in N-values between them widens for D_r larger than around 50%. Combining the finding that N-values of well-graded gravels are considerably larger than that of poorly-graded sands for the same D_r for D_r>50% with the triaxial test results shown in Figure 16 (a) that the CRR-values of granular soils are almost uniquely determined by relative density D_r may explain the reason why the CRR-values of well-graded gravels shown in Figure 15 (a) were much lower than those of poorly-graded sands under the same SPT N_1–value for N_1> 25-30.

On the other hand, Figure 16 (b) exemplifies the deviatoric stress/pore-pressure versus axial strain relationship obtained in undrained monotonic loading tests carried out just after the cyclic loading for the three soils, RS1, RS2 and RS3 with relative densities D_r≒50%. In the cyclic loading tests, all specimens attained about 10% DA axial strain and hence were already liquefied according to

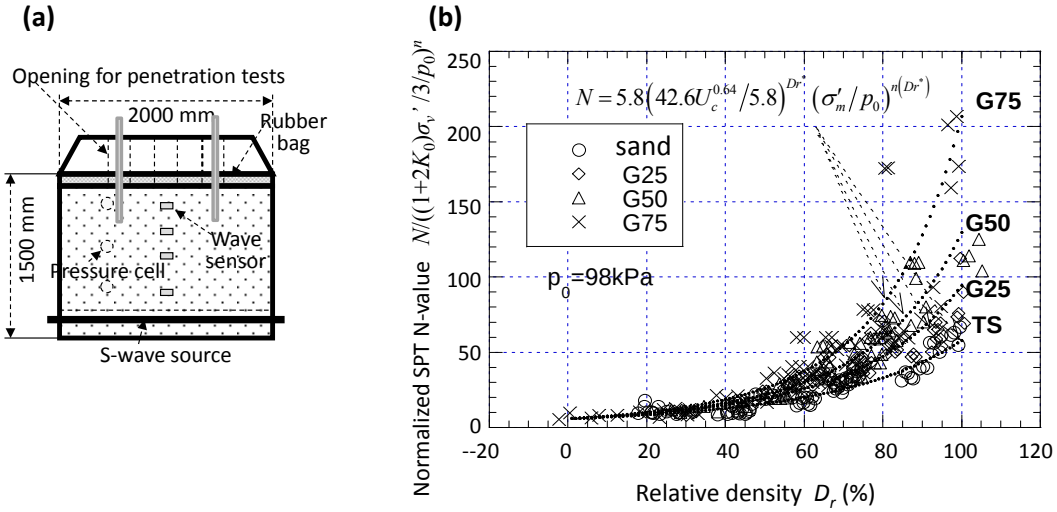

Figure 17. Calibration chamber tests for sands and gravels: (a) Pressurized soil container for SPT, (b) Normalized SPT N-values versus D_r for 4 soils with different particle grading (Kokusho 2007).

the normal engineering practice. In response to the monotonically increasing strain, the deviatoric stress and the pore pressure rise gradually up to some asymptotic values. It is remarkable that despite almost the same D_r-value, mobilized stresses are quite different among the three soils; the well-graded gravel RS3 tends to exhibit a much higher shear resistance than the poorly-graded sand RS1. Thus, it can be said that well-graded gravelly soils are as prone to liquefaction as poorly-graded sands in terms of 5% DA axial strain, if their relative density is the same as shown in Figure 16 (a). However, if shear resistance at a strain much larger than 5% DA strain (equivalent to 2.5% single amplitude strain as illustrated in Figure 16 (b)) is considered, the relative density is no longer a relevant scale. Instead, the particle gradation represented here by the uniformity coefficient C_u makes a big difference even for soils of the same relative density. This implies that well-graded gravelly soils are less prone to post-liquefaction failure inflicting large deformation. Considering that the C_u–values of natural gravelly soils are normally as large as several tens as indicated in Figure 14 (a), their post-liquefaction undrained strength corresponding to 25% axial strain may be judged at least 8 times larger than poorly-graded sands according to Figure 16 (b). Thus, post-liquefaction large ground deformation such as cracks, differential settlements and lateral spreading seems to be harder to develop in well-graded soils than in poorly-graded sands of the same D_r, even though the initial liquefaction with almost 100% pressure buildup or $\varepsilon_{DA} = 5\%$ strain is attained as easily as sands. This observation, also considering that the N_1 versus D_r correlation is not so much different between gravels and sands for N_1< 25-30 as shown in Figure 17 (b), can presumably explain why the CRR-values for gravels are higher than those of sands for the same SPT N1-value in Figure 15 (b). This is because the CRR-values in Fig. 15 (b) reflect the shear resistance at strains inducing fissures and lateral spreading much larger than $\varepsilon_{DA} = 5\%$, which is significantly higher for well-graded gravels than sands as demonstrated in Figure 16 (b).

The above observations were all based on test results on clean sands and clean gravels without fines. Because granular soils become distinctly contractive with increasing fines content not only for sands but also for gravels, the post-liquefaction shear resistance tends to decrease drastically as F_c increases from F_c=0 to the critical fines content CF_c, where the fines start to overflow the

voids of gravel particles, thus changing the soil structure from gravel supporting to matrix-supporting (Kokusho 2007). In addition to fines content, the crushability of coarser gravels may also considerably reduce not only the liquefaction resistance but also the post-liquefaction shear resistance of gravelly soils (Hiraoka 2000). It may well be that the liquefaction in Kobe's reclaimed land areas during the 1995 Kobe earthquake caused considerable large deformation damage in gravelly fills because the liquefied decomposed granite soils were rich in non-plastic fines and the gravel particles were crushable due to strong weathering in granite rocks.

Lateral Spreading under Initial Shear Stress

As already mentioned, a simplified in situ stress condition of a soil element consolidated under K_0 conditions and cyclically sheared without sustained initial shear stresses (i.e. level ground) has been the standard model for evaluating liquefaction triggering mechanisms in engineering practice (Seed and Lee 1966). Needless to say, sands tend to deform laterally and spread during liquefaction when under the influence of initial shear stresses, and this has caused significant damage to earth dams, superstructures and buried life lines, sometimes with a time delay. The sliding of the lower San Fernando dam, in particular, highlighted the significance of this failure type (Seed 1987). The mechanisms that lead to such large lateral displacements are still only poorly understood and how to logically design for these effects is quite controversial.

In this respect, Casagrande (1971) provided a completely different view on the liquefaction mechanism focusing on the role of sustained initial shear stress in near slopes and superstructures as illustrated in Figure 18 (a). He proposed use of the term "liquefaction" for a phenomenon in which a contractive sand loses its shear strength, not necessarily by cyclic loading but by monotonic loading, and undergoes a flow-type failure when the reduced strength is lower than the initial static shear stress. Accordingly, the term "cyclic mobility" was proposed for the zero effective stress condition in a dilative sand by cyclic loading. The same author, followed by Castro (1975), utilized the concept of the steady state line (SSL) to illustrate these concepts, as shown on the void ratio e versus effective confining stress σ_c' plane in Figure 18 (b). In this "state diagram", liquefaction is interpreted as the result of undrained failure of a saturated loose contractive sand; for example,

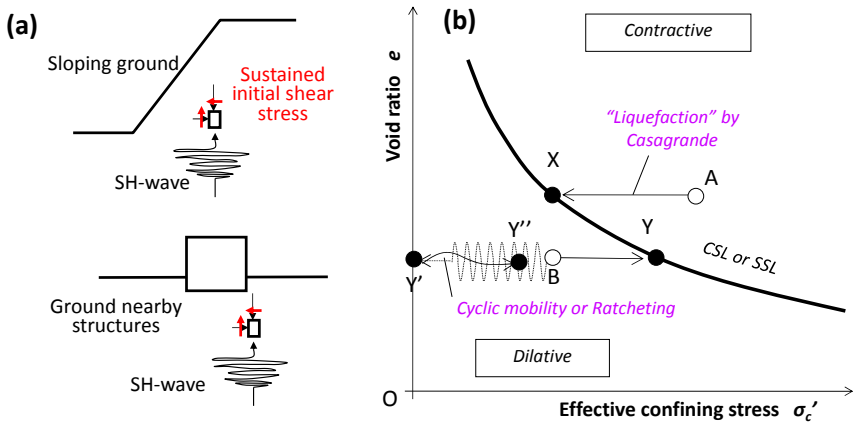

Figure 18. Soil elements prone to lateral spreading under sustained initial shear stresses (a), and $\sigma_c' \sim e$ state diagram and CSL (Critical State Line) or SSL (Steady State Line) dividing into contractive and dilative states (b).

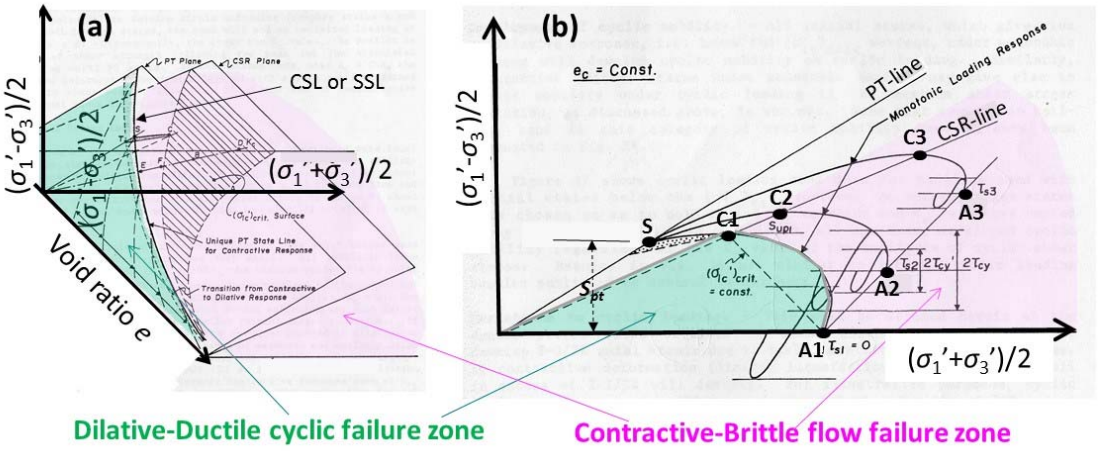

Figure 19. Three-dimensional effective stress diagram ($e \sim (\sigma_1'+\sigma_3')/2 \sim (\sigma_1'-\sigma_3')/2$) (a), and a typical section ($(\sigma_1'+\sigma_3')/2 \sim (\sigma_1'-\sigma_3')/2$) at constant void ratio e (b) (modified from Vaid & Chern 1985).

a loose sand starting at point **A** and eventually ending with steady-state flow at constant volume at **X** on the SSL. If a dilative sand is monotonically loaded starting at **B** in the undrained condition, the point moves right toward **Y** on the SSL with increasing effective confining stress σ_c'. If the same sand is loaded cyclically, the point moves from **B** to the left due to negative dilatancy during cyclic loading and eventually reaches zero-effective stress at point **Y'** under the zero-shear stress condition (in a level ground). However, subsequent undrained monotonic loading translates the state point to the right to **Y''** and the resistance of the specimen increases again.

In order to merge the two different views of Seed and Casagrande, Vaid & Chern (1985) systematically performed triaxial tests to illustrate "a unified picture of the undrained monotonic and cyclic loading response of saturated sands" including the effect of initial shear stress in cyclic loading tests. Figure 19 (a) shows a three dimensional effective stress diagram in $e \sim (\sigma_1'+\sigma_3')/2 \sim (\sigma_1'-\sigma_3')/2$ space, which is an extension of the state diagram shown in Figure 18 (b). Figure 19 (b) shows a typical section ($(\sigma_1'+\sigma_3')/2 \sim (\sigma_1'-\sigma_3')/2$) at a constant void ratio e, where stress paths for monotonic as well as cyclic loading are drawn starting from points A1, A2, A3 with different initial shear stresses $(\sigma_1'-\sigma_3')/2$, with σ_3'=constant. For monotonic loading, a contractive flow-type failure (liquefaction or limited liquefaction in the Casagrande's definition) is triggered at Points C1, C2, C3 on a straight line (called CSR-line) shown in the figure, only if the starting points A1, A2, A3 are on the contractive side of the 3-dimensional state diagram. The CSR-line is uniquely defined for stress paths of a given sand to have peak values and initiate strain softening thereafter. During strain softening, the sand undergoes flow deformation followed by subsequent strain hardening at Point S (if the flow is a limited type), which is on the PT (phase transformation)-line defined by Ishihara et al. (1975). Another important condition for a contractive sand to undergo flow type failure is that the shear stress $(\sigma_1'-\sigma_3')/2$ on the CSR-line (at Point C3 for example) should be larger than that at S (S_{PT}) so that the stress path can undergo strain softening after reaching the peak (Vaid & Chern 1985).

In the case of cyclic loading under sustained initial stress, Vaid and Chern (1985) demonstrated

that the condition for the occurrence of flow-type failure is the same as for monotonic loading. Namely, stress-paths starting from points A1, A2, A3, superposed in Figure 19 (b) should come across the CSR-line at a point with the shear stress higher than the stress S_{PT} of Point S, so that the sand undergoes the flow-type or limited flow-type failure. One significant difference from monotonic loading is that cyclic loading builds up the pore-pressure, which pushes the effective stress path to the CSR line and enables the flow-type failure to occur with a shear stress (initial + cyclic stress amplitude) smaller than that (initial + static shear stress) in monotonic loading even though starting from the same A1, A2, A3. If any of the conditions necessary for triggering flow-type or limited flow-type failure mentioned above is not met, then sand exhibits cyclic mobility in which strains tend to develop gradually in a ductile failure mode. In contrast, flow-type failures may develop infinitely large or large but limited strain quite abruptly leading to a dangerous brittle failure mode in liquefied ground with sustained initial stresses. Although other research on mechanical models has been performed besides Vaid & Chern (1985) to obtain similar findings (e.g. Sladen et al. 1985, Alarcon-Guzman et al. 1988), issues associated with how to evaluate residual deformation depending on the failure types have to be agreed upon before establishing a unified liquefaction design practice that considers the effect of initial shear stress.

In many previous undrained shearing test results on clean sands, a typical flow type response with a peak strength followed by steady-state or residual strength for infinitely large strain was not often observed. Instead, limited flow-type failure is more often observed. This is characterized by a temporary quasi-steady state strength followed by regaining shear resistance with further straining. For example, Ishihara (1993) made a comprehensive database of sand behavior in undrained monotonic loading from laboratory tests. Figures 20 (a), (b) depict the undrained behavior of clean Toyoura sand with D_r=38% under various effective confining stresses. The relatively loose sand is obviously dilative for the confining stress σ_c'=0.1 Mpa and starts to be slightly contractive for σ_c'=2.0 Mpa or higher by showing a temporary reduction after a peak in the deviator stress $q = \sigma_1' - \sigma_3'$ and an increase again as the limited flow-type failure. In contrast to a steady state flow with infinitely large strain, this response was called limited liquefaction by Casagrande (1975) and the temporary minimum value was termed the quasi-steady state strength (Alarcon-Guzman 1988, Ishihara 1993). In normal liquefaction problems for shallow depths less than 10m, the relative density of loose sand deposits is around D_r=30-40% as in Niigata city and the effective confining

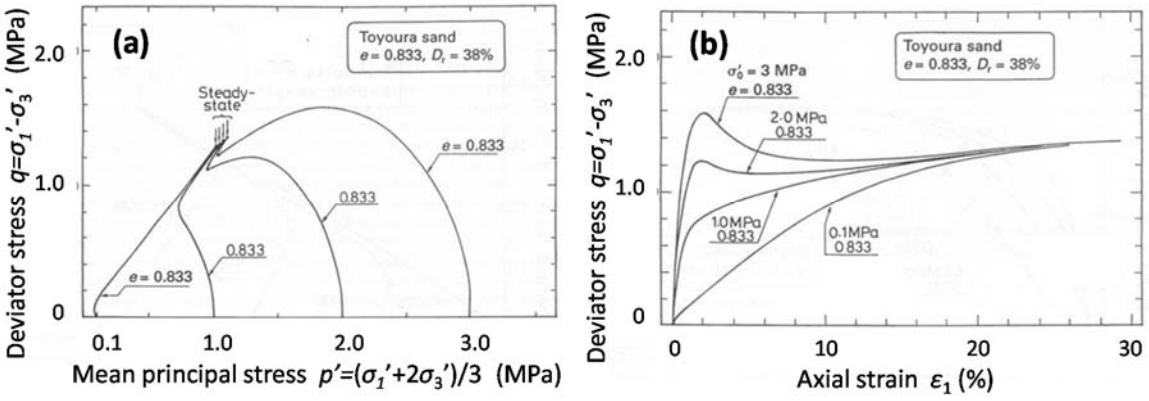

Figure 20. Undrained monotonic loading test results of D_r=38% Toyoura sand under different initial confining stress: (a) Effect stress paths, (b) Stress versus strain curves (Ishihara 1993).

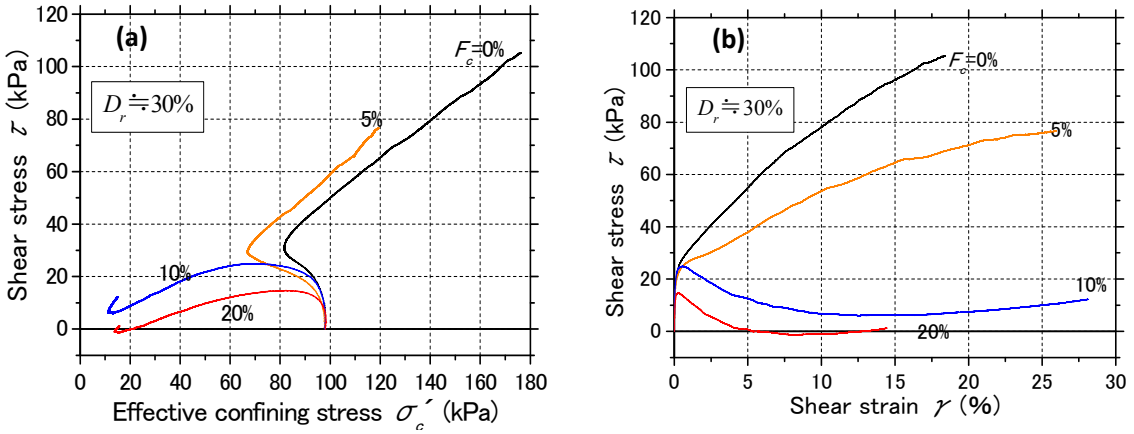

Figure 21. Increasing contractive behavior of Futtu sand with increasing non-plastic fines, F_c=0~20% by torsional shear tests: (a) τ~ σ_c', (b) τ~ γ (Kusaka 2013).

stress is σ'_c=0.1 Mpa or lower, indicating that clean sand is always on the dilative side and the flow-type failure (even limited flow type) seems to be difficult to occur based on the results in the laboratory tests. However, the presence of low/non-plastic fines mixed with clean sands changes the volume change behavior significantly.

The significant role of fines in reducing the shear-induced dilatancy of clean sands was pointed out by several researchers (e.g. Ishihara 1993). Figure 21 shows a typical example of undrained monotonic loading torsional shear tests on loose sand specimens with parametrically increasing non-plastic fines under an isotropic effective confining pressure σ'_c=98 kPa (Kusaka 2013). For

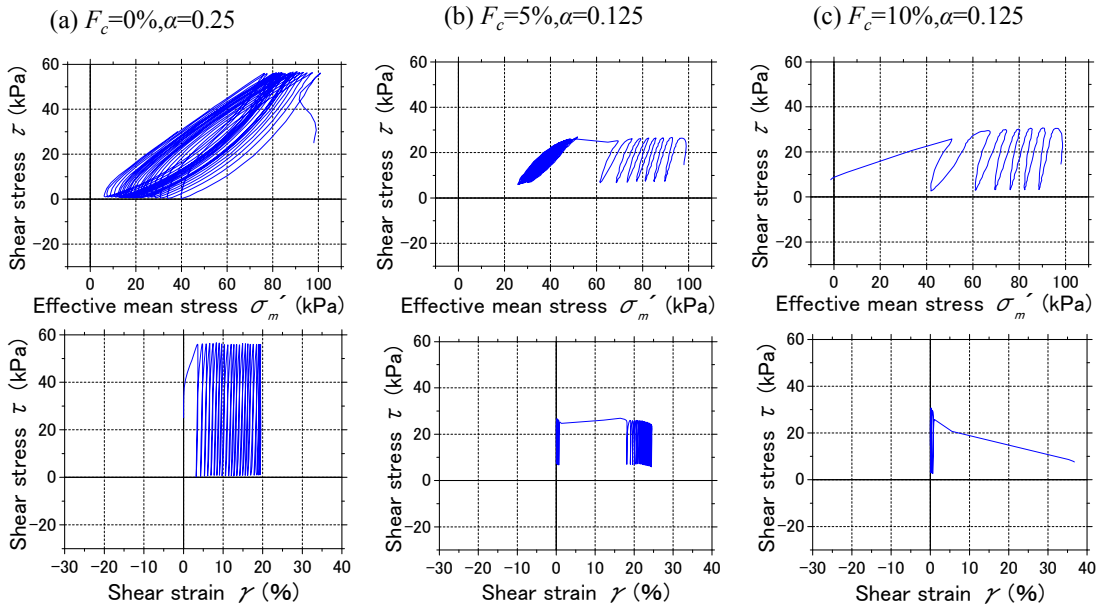

Figure 22. Torsional cyclic loading test results of D_r≒30% under initial shear stress: (a) Futtu sand F_c=5% with cyclic gradual failure, (b) F_c=5% with limited flow failure, (c) F_c=10% with unlimited flow failure (Arai 2014).

the same low values of relative density D_r≒30%, the clean sand of F_c=0 is clearly dilative, while it becomes contractive with limited flow for F_c≥10% and exhibits perfect flow with almost zero residual strength for F_c=20%. This is presumably because the steady state line is significantly influenced by F_c, and contractive and dilative zones on the state diagram change drastically (e.g. Papadopoulou, A. and Tika, T. 2008).

In accordance with the monotonic loading tests, Figures 22 (a)~(c) compares test results of undrained cyclic torsional shear tests on the same sand samples as in Figure 21 with parametrically varying non-plastic fines under an initial shear stress ratio $\alpha = \tau_s / \sigma_c'$ =0.125 or 0.25 and σ_c'=98 kPa. For the clean sand with α =0.25 (a), the pore-pressure and associated strain tends to increase only gradually up to limited values due to the no stress reversal condition making the failure very ductile, because the clean sand is dilative as indicated by monotonic loading in Figure 21. For the case of F_c=5% with α =0.125 (b), a gradual increase of strain in the initial stage is followed by a limited flow failure and then a convergence to an ultimate value, presumably reflecting a slight contractiveness of the sand. For the case of F_c=10% with α =0.125 (c), a large strain occurs in the flow-type failure making the failure very brittle, because the sand with this F_c-value responds contractively as observed in the monotonic loading. Though the effect of F_c appears to be slightly different in Figures 21 and 22, its enormous influence on the liquefaction failure is obvious in both monotonic and cyclic loading tests.

In current engineering practice, the effect of initial shear stress is considered to be one of the influencing factors on liquefaction triggering. For example in North American practice, a parameter $K_\alpha = CRR_\alpha / CRR_{\alpha=0}$ is used (Idriss & Boulanger 2008), where CRR_α is the cyclic resistance ratio under initial shear stress ratio $\alpha = \tau_s / \sigma_v'$ (τ_s =initial shear stress, σ_v'=effective normal stress). The effect of initial shear stress on the liquefaction triggering was first investigated using a ring-shear apparatus by Yoshimi & Oh-oka (1975), who found that for dilative sands it is important for the shear stress (initial shear stress + cyclic shear stress) to reverse plus and minus (stress reversal) for 100% pressure buildup. In contrast, Vaid & Chern (1983), by conducting cyclic triaxial tests on anisotropically consolidated specimens, showed that even without the stress reversal, liquefaction strength tends to reduce with increasing α if the sand is loose enough to be contractive.

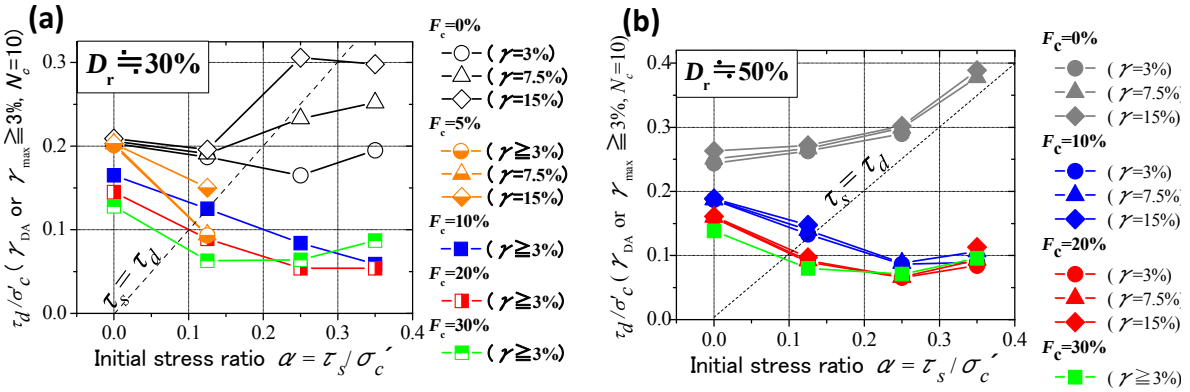

Figure 23. Variation of CRR with increasing initial shear stress ratio α for sands of various fines content F_c=0~30%: (a) D_r≒30%, (b) D_r≒50% (Arai et al. 2014).

Figure 23 shows torsional shear test results on sands of D_r≒30% and 50% with non-plastic fines, F_c=0~30%, isotropically consolidated by σ_c'=98 kPa and loaded by cyclic shear stress τ_d in the undrained condition under sustained initial shear stress τ_s. The CRR-values defined for shear strain γ=3, 7.5, 15% in the number of cycles N_c=10 are plotted versus increasing initial shear stress ratio $\alpha = \tau_s / \sigma_c'$. The enormous effect of F_c on the α -dependent CRR variations is quite obvious for D_r≒30% and 50% as well, because the fines tend to change the behavior of the clean sand from dilative to contractive as already seen. The diagonal dashed line corresponding to $\tau_s = \tau_d$ in the chart also influences liquefaction behavior; above the line ($\tau_d > \tau_s$) the stress reversal tends to make pore-pressure buildup easier and lowers the CRR-values. For dilative sands of F_c=0 and D_r=50% in particular, the CRR-value tends to increase with increasing α even in the stress reversal condition. In contrast, for contractive sands with F_c ≥5~10%, the CRR-values tends to decrease in most cases despite the non-stress reversal conditions; this is consistent with Vaid and Chern (1983). Also note that all the plots for γ=3% to 15% are almost overlapping and make a unified curve, indicating that the liquefaction-induced flow failure tends to develop very rapidly even in the non-reversal condition for contractive sands containing fines. In contrast, liquefaction in clean sands is triggered more easily in a level ground free from any initial shear stress than those in nearby shallow foundations or slopes.

In liquefaction-related design, the flow-type brittle failures accompanying a sudden increase of limited or unlimited large strains are far more important and need greater care than non-flow type ductile failures with gradually increasing cyclic strain. In the case of non-flow failure, the design concern is how to evaluate the cyclic strain accumulation and compare that with design values corresponding structural performances. In the flow-type failures, a critical evaluation of soil stability (Vaid & Chern 1985) is needed because the induced strain is almost unlimited and difficult to predict. It is thus immensely important to establish a reasonable liquefaction-related design methodology covering all the failure types from the viewpoint of PBD.

Lateral Flow by Void Redistribution

In the author's view, the most difficult in situ behavior to reproduce in laboratory soil element tests is a lateral flow in gentle slopes as observed in Niigata city during the 1964 Niigata earthquake. Figure 24 (a) shows an area in Niigata city near the Niigata railway station where a lateral flow exceeding 4m of horizontal displacement occurred in a loose sand deposit with SPT N_1-value=9 on average despite the very gentle slope of 1% or less. The elevation contours of 0.1m increment are superimposed on the map (Kokusho & Fujita 2002). It is noted that the displacement vectors measured by Hamada (1992) are pointing down-slope and are mostly normal to the elevation contours. Borehole logging data compiled along the solid lines, L1 and L2 shown on the map, indicated that the soil essentially consists of loose clean sands sandwiching one or more fine soil sublayers. The flow displacements D_{fn} in this area are plotted versus the maximum surface inclinations normal to the contours, β_{max} with open symbols in Figure 24 (b). The plots enclosed in the diagram seem to indicate the existence of a close correlation between D_{fn} and β_{max} despite large data scatter. However, the correlation in the other area shown with solid symbols differs, and

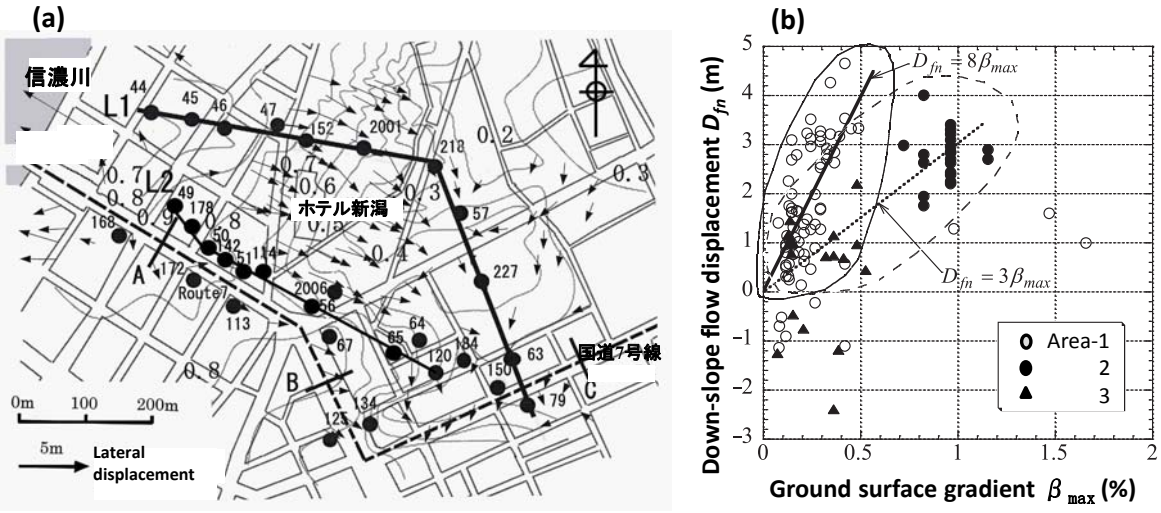

Figure 24. Lateral flow in Niigata city in a very gentle slope: (a) flow vector compared with elevation contours of 0.1m pitch, (b) surface gradient versus flow displacement plots (Kokusho & Fujita 2002).

likely reflects different soil conditions. Shear strains concentrated in liquefied layers were evaluated as 20~200% (kokusho & Fujita 2002). Thus, even a slight surface inclination of less than 1% seems to have had a great influence on the flow displacement in Niigata city. None of the undrained shear mechanisms seems to explain the large residual strain that occurred there with the working initial shear stress of around 1% (initial shear stress ratio $\alpha = \tau_s / \sigma'_v$ =0.01) or lower. Furthermore, the sand was definitely clean with fines content less than a few percent as shown in Figure 26 (c), and was actually no looser than D_r=30% (Kamikawa 2004) under confining stresses no higher than σ'_c=98 kPa.

A similar failure mechanism in liquefied deposits seems to be involved in seismically-triggered near-shore submarine slides. The slope gradients in those slides are normally only a few degrees or even less. For example, the port city of Valdez in Alaska, USA, suffered great loss of human lives and property by large scale coastal submarine slides during the 1964 Alaskan earthquake (Coulter et al., 1966). As shown in Figure 25 (a),

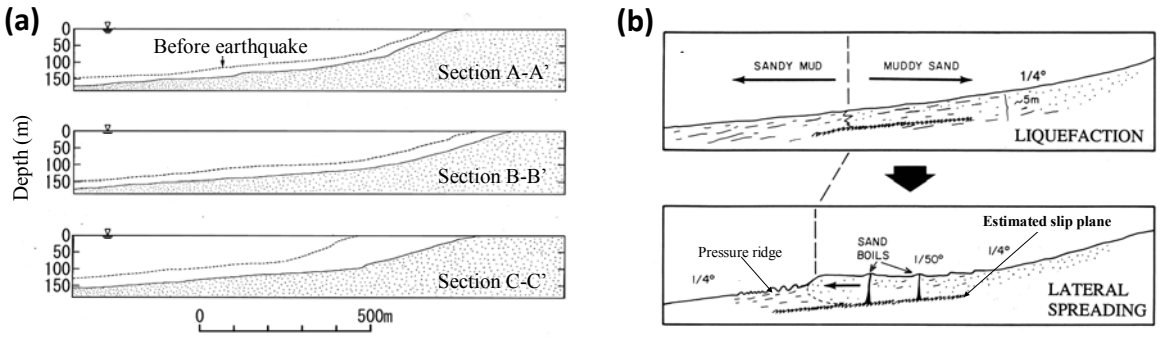

Figure 25. Cross-sectional change of sea bed before and after seismically induced submarine slide: (a) Valdez during the 1964 Alaskan earthquake (Coulter et al., 1966) , (b) Off-California Coast during 1980 medium Magnitude earthquake (Field et al. 1982).

the inclination of the sea bed consisting of glacially deposited silty sand was 5° or less on average for a long span of the slip surface of more than 2 km offshore. Another typical submarine slide occurred 60 km off the California Coast during a 1980 medium magnitude earthquake was well investigated (Field et al. 1982). A seabed with a gradient of only 0.25 degrees, extending horizontally 2 by 20 km and consisting of interbedded sand and mud sublayers, slid and became almost flat with clear evidence of liquefaction such as sand boils on the sea floor in 30 to 70 m water depth as sketched in Figure 25 (b).

Different from mechanical models on uniform sand, a partially drained mechanism using the terminology "water interlayer" was addressed in a committee report in US (National Research Council, 1985), though this concept seems to have been intuitively shared among geotechnical engineers and researchers even before that. Namely, fine soil sublayers or seams sandwiched in sand deposits are considered to play a key role in flow failures as illustrated in Figure 26 (a).

Soil stratifications were investigated in situ by utilizing dewatered trenches at 2 sites in Japan (Kokusho and Kojima, 2002): a hydraulically filled deposit along Tokyo Bay and a natural sand deposit in Niigata city where extensive liquefaction occurred during the 1964 Niigata earthquake. Figures 26 (b), (c) show the sieving test results conducted in the two sand deposits by thin slices of 2 cm vertical thickness. The percentage finer by weight in different mesh sizes is plotted versus elevation. In the reclaimed deposit, the soil is highly variable and the fines content F_c corresponding to the mesh size of 0.075 mm (#200 sieve) is fluctuating almost periodically by an interval shorter than 2 m, with contents of other particle sizes changing accordingly. These fine soil sublayers were observed from horizontal stripes along the trench slope to be continuous to some extent. Normal borehole logging is likely to miss such alternating thin fine layers and misinterpret the soil as uniform silty sand. In Niigata, the soil is rather uniform, consisting of clean sand down to elevation -5.6 m, and below that a silty or clayey layer about 0.6 m thick and a humus layer 15 cm thick appear. These low-permeability layers were confirmed to be continuous in the horizontal

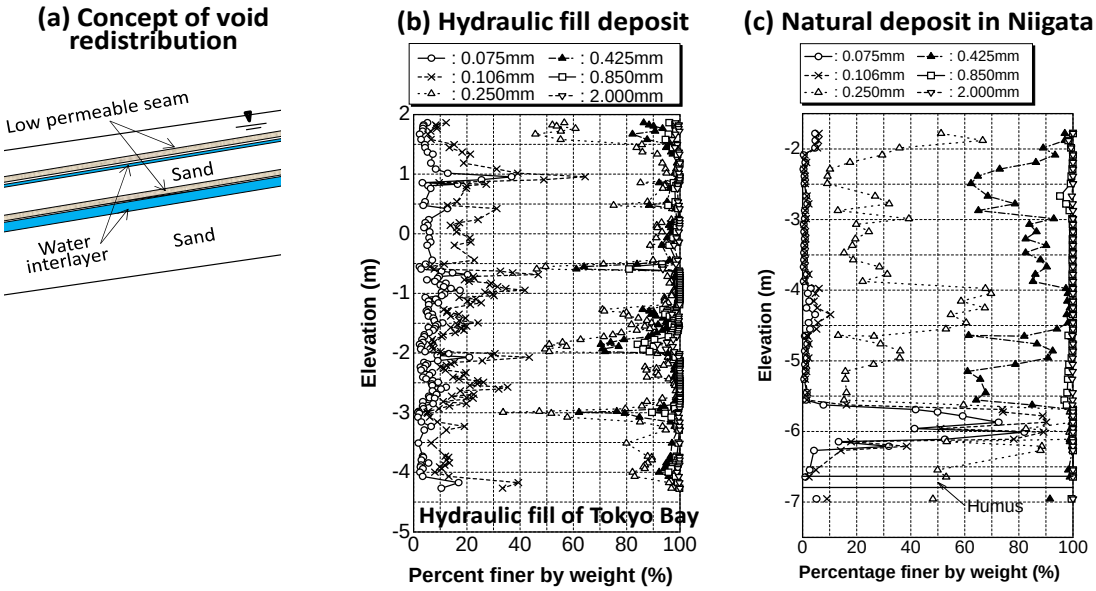

Figure 26. Concept of void redistribution (a), and sieving test results at two sites, hydraulic fill deposits (b) and natural sand deposits (c). (Kokusho 2003).

direction to at least 20 m. It may be expected that the interbedded silty sublayers result in differences in permeability in liquefied sand, causing void redistribution in the form of water interlayers or water films.

The formation of water films in liquefied sand beneath low-permeability seams was observed in a number of one-dimensional model tests (e.g. Scott and Zuckerman 1972, Elgamal et al. 1989, Kokusho 1999). The test results clearly indicated that a water film is readily formed after the onset of liquefaction of loose sands beneath a sandwiched seam of lower permeability because of pore-water migration or void redistribution and stays there much longer than the re-sedimentation of liquefied sand particles. This inevitably brings about a sort of instability in liquefied ground if the ground is inclined even very gently. Naesgaard & Byrne (2005) suspected that another mechanism, called "soil mixing," may also be involved, leading to significant strength reduction along a silt seam if the grain-size ratio between sand and silt satisfies a certain condition of mixing.

Two-dimensional shake table tests were also performed, in which a saturated loose sand slope of $D_r \fallingdotseq 30\%$ was made in a rectangular soil box and an arc-shaped non-plastic silt seam was sandwiched in it as shown in Figure 27 (a) (Kokusho 2003). In the time histories of flow deformations at the target points shown in (b), the flow occurred only during shaking if there is no silt seam (c), while much larger post-shaking flow occurred with a clear delay time in the case with the silt seam even with smaller shaking table acceleration (d). Kokusho (2006) found in several different test conditions that the post-shaking flow displacement tended to be much larger than that during shaking. Kulasingam et al. (2004) and Malvick et al. (2005) demonstrated that the strain concentration

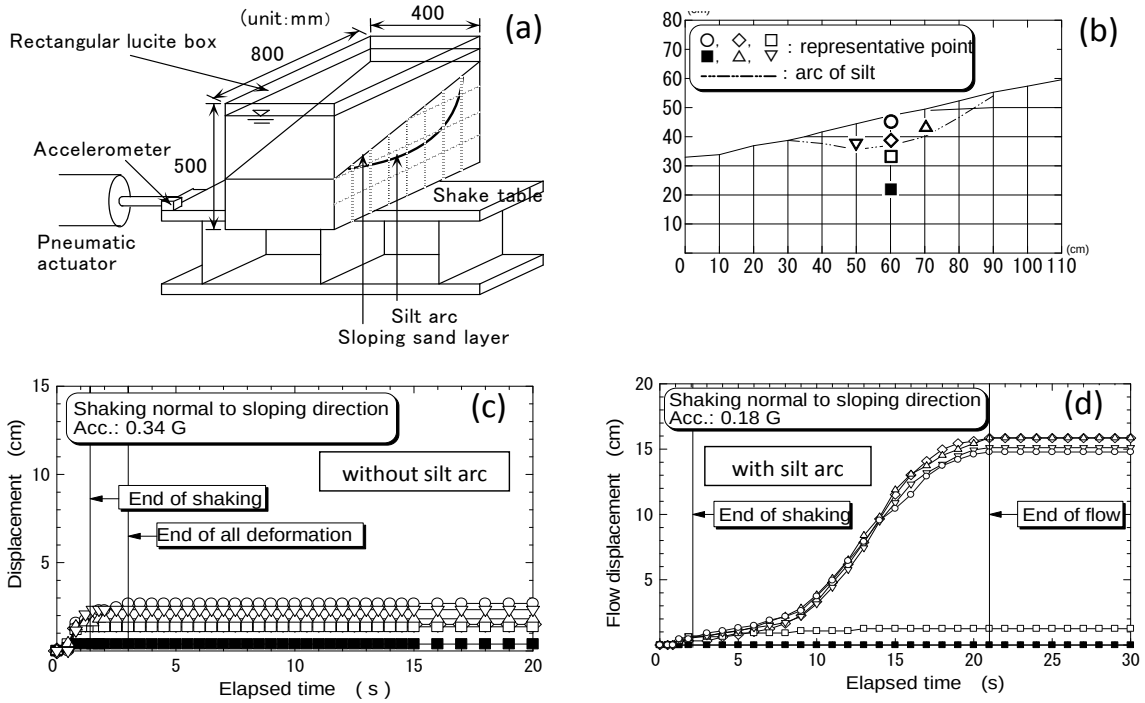

Figure 27. Two-dimensional shaking table test on model slope: (a) a test setup for saturated sand slope without/with a silt arc, (b) target points,(c) time histories of displacements without silt seam, (d) with silt seam (Kokusho 2003).

along a low-permeable seam and delayed slip occurs also in centrifuge model tests and showed the potential importance of various factors such as shaking intensity and duration, layer thickness, permeability contrasts, etc.

A question may arise as to why clean sand, which is actually on the dilative side of the state diagram, does not absorb ambient excess pore-water but allows a water film to develop after shaking. It has been shown based on a comparison of cases with and without a silt seam (Kokusho, 2003) that a water film, once formed beneath the seam, serves as a shear stress isolator which shields the deeper soil from the initial shear stress in a sloping ground and hence from the development of shear strain and dilatancy. Consequently, the clean sand can undergo large shear strain beneath the silt seam without the dilative behavior in ultra-low effective confining stress after the formation of a water film as shown in Figure 26 (d). In contrast, uniform sands stop flowing immediately after the end of shaking as in Figure 26 (c) because the sand behaves dilatively. If water films are continuous over a large lateral extent, and sliding can occur all the way through a continuous water film, the residual strength would be zero. The strength actually evaluated during the delayed flow along the water film in the above-mentioned model test was around 20% of the shear strength of the uniform sand, being almost independent of the sand density and other test parameters (Kokusho 2006). This is probably because sliding through a water film tends to start as soon as the mobilized shear stress exceeds the resistance, keeping the sand beneath the water film slightly dilative because of imperfect shear stress shielding due to imperfect development of the water film.

The post-liquefaction void-redistribution mechanism in a sloping sand layer was investigated in the light of soil behavior observed in volumetric-strain-controlled triaxial tests with constant shear stress (Boulanger and Truman 1996). A submerged infinite gentle slope of liquefied sand capped by a low-permeability layer is schematically illustrated in Figure 28 (a), wherein the upward flow of pore water due to the earthquake-induced excess pore-pressures leads to dilation of the sand

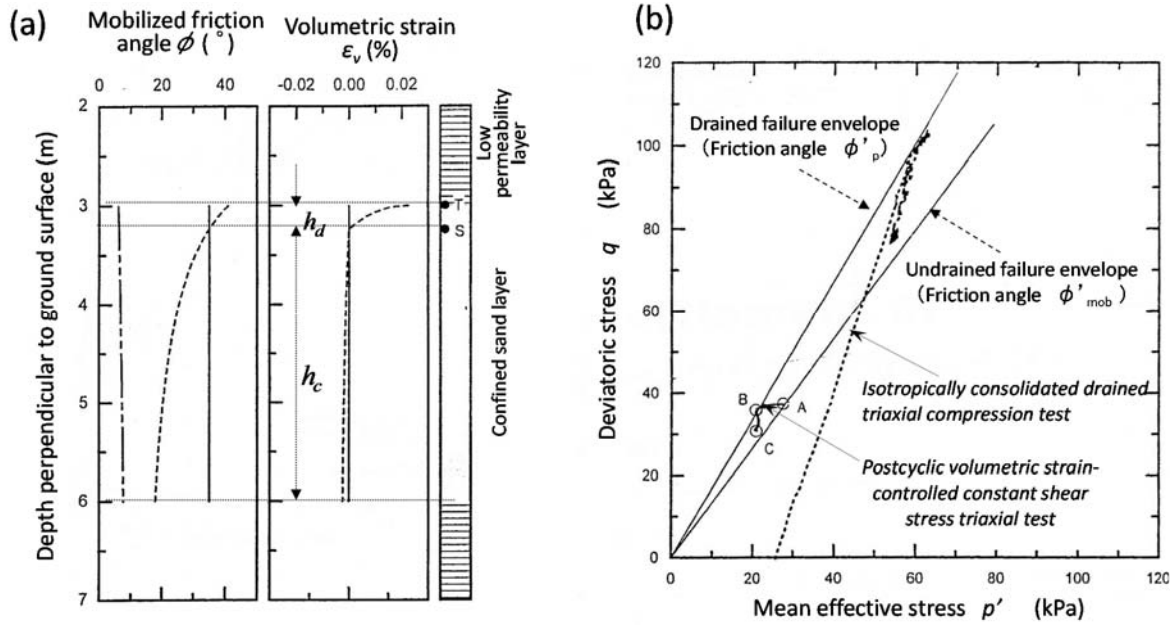

Figure 28. Void redistribution mechanism simulated in triaxial tests: (a) an infinite sand slope capped with low permeability layer, (b) effective stress path in post-cyclic volumetric strain-controlled constant shear stress test (modified from Boulanger & Truman 1996).

near the upper boundary with the thickness h_d. The soil with the thickness h_c below this zone contracts as there is a net outflow of water upward towards the dilating zone. The inflow of water from below will dilate the sand in the dilating zone and raise the pore pressure to a maximum value corresponding to a peak friction angle ϕ'_p shown on the *p'-q* chart in Figure 28 (b). The corresponding friction angle (initially ϕ'_{mob} for undrained condition; Point A) increases up to the peak friction angle ϕ'_p for the drained condition (Point B). This allows the dilating zone to absorb the incoming water to a certain extent. Further continued inflow of water would then reduce the pore-pressure toward the value corresponding to the steady state line (Point C). When an element in the dilating zone has reached the steady state, its steady state strength, if it were loaded undrained at this time, would be equal to the driving shear stress acting parallel to the ground surface. Any further inflow of water to the dilating zone would cause instability of the slope, because with no further dilation being possible the water film will be formed leading to instability of the slope as discussed above. Based on the above-mentioned analysis on the post-liquefaction void redistribution process, Boulanger and Truman (1996) also indicated a procedure to evaluate the thickness of dilating zone h_d and threshold thickness of the contracting zone h_c for triggering instability by comparing the maximum volumetric increase in h_d (V_{dil}) with the volumetric decrease due to consolidation in h_c (V_{con}). If the thickness of the contracting zone h_c is larger than those, then $V_{dil} < V_{con}$, and instability is likely to occur in such a way that excess pore water concentrates at the top of the dilating zone and forms a water film.

Void redistribution has drawn increasing attention in recent years. More research efforts are needed to integrate such findings into actual design methodologies, though it may not be easy due to in situ complex soil stratifications. In this respect, Seed (1987) summarized case history data of lateral flow or lateral spreading and proposed an empirical relationship between the back-analyzed residual shear strength and corresponding in situ penetration resistance. Comparing with the relationship based on undrained laboratory tests, it was found that the residual strength estimated from the case studies gave significantly lower strength presumably due to void redistribution or partial drainage effect in stratified heterogeneous soil in situ. Similar back-calculations from actual case histories of lateral flow failures have been implemented by quite a few investigators since then in North America (e.g. Olson and Stark 2002), in which residual shear strength normalized by vertical effective stress was correlated with normalized SPT blow counts $(N_1)_{60}$. Despite considerable scatter in the data points in such studies, which reflects the complexity involved in in situ flow failure mechanism including void redistribution, $(N_1)_{60}$ values in the majority of the previous flow failure cases are lower than 10~12, indicating that this type of failure seldom occurred in soils denser than that.

A numerical study has been performed of the lower San Fernando dam failure and a submarine slide model test in order to evaluate whether the effect of void redistribution can be properly simulated (Naesgaard et al. 2009). It showed that post-liquefaction displacements were much larger when void redistribution was considered. However, it is still a difficult task to delineate a simple and reliable methodology that accounts for void redistribution for actual designs. More quantitative research on detailed case histories, sophisticated model tests and analytical efforts are needed to evaluate flow deformation for a variety of soil conditions and to predict the flow displacement.

Concluding Remarks

In the past half century, considerable effort has been made in liquefaction research from laboratory studies to understand the basic mechanisms of liquefaction and compare those results with in situ liquefaction behavior from case histories of previous earthquakes. Both liquefaction triggering and liquefaction-induced deformations have been studied for performance-based design in geotechnical engineering. However, in view of recent liquefaction cases, several issues are still require further clarification.

1. Besides relative density, the significant effect of soil fabric on liquefaction triggering has been well recognized among engineers. In this respect, long-term geological effects including cementation are reflected in soil fabric and affect liquefaction resistance, which is difficult to quantitatively detect in the current state of art. These aging effects have been observed during recent earthquakes particularly in Japan. How to consider aging effects in evaluating liquefaction potential in various depositional environments based on penetration tests combined with other in situ parameters is one of the important topics to investigate further.
2. The plasticity index of fines I_p or clay content C_c has been identified as a more significant parameter than fines content F_c in evaluating the liquefaction potential of silty sands. In Japan, $I_p \leqq 15$ or $C_c \leqq 10\%$ is normally used for an initial screening for liquefaction. However, during the 2011 Tohoku earthquake, extensive liquefaction occurred in the Tokyo bay area in soils including highly plastic sublayers interbedded with low-plasticity sublayers, erupting a large amount of non-plastic ejecta on the ground surface. Thus, liquefaction susceptibility of interbedded layers with low and high plasticity needs further examination on the effects of I_p or C_c on global liquefaction susceptibility.
3. Gravelly soils are normally well-graded and considered to have higher liquefaction resistance than poorly-graded sandy soils for the same relative density D_r. This perception seems to come from the fact that the undrained shear resistance of gravelly soils corresponds to a strain level much higher than that of the onset of liquefaction. If the strain level for liquefaction triggering (5% DA strain) is considered, the cyclic resistance ratio obtained is almost the same as for poorly-graded sands of the same D_r. In evaluating liquefaction susceptibility of gravelly soils, one should be conscious of the induced strain level to be considered in the engineering design.
4. For establishing performance-based design in geotechnical engineering, soil behavior under initial shear stress after triggering liquefaction needs to be investigated further. A unified evaluation method for liquefaction triggering and post-liquefaction deformation under sustained initial stresses has to be developed considering the state diagram and the effects of cyclic loading effect. In this respect, the significant effect of non/low-plastic fines, which tends to drastically reduce soil dilatancy, should be considered.
5. Lateral flow involving water films due to void redistribution in layered loose sands seems to be a mechanism which can exclusively explain flow failure in gently inclined liquefied clean sand deposits such as in Niigata. Water films developed beneath low-permeability silt seams are likely to play a major role in a delayed flow failure in many case histories of lateral flow failures. Despite the significance of this failure, it may not be easy to account for this effect in engineering design, because it is hard to construct exactly 2 or 3-dimensional map of low-permeability seams. Technical advances in in situ soil investigations, modelling and numerical analyses are needed to take this effect quantitatively into design practices.

Acknowledgments

Professor Christopher Baxter, University of Rhode Island, USA, and Dr. Ernest Naesgaard, Geotechnical Engineer in British Columbia, Canada are gratefully acknowledged for their great help in editing the final manuscript thoroughly.

References

Alarcon-Guzman, A., Leonards, G. A. & Chameau, J. L. (1988): Undrained monotonic and cyclic strength of sands, *J. Geotech. Eng.* ASCE, 114, GT10, 1089-1109.

Andrus. R. D. and Youd, T. L. (1989): Penetration tests in liquefiable gravels, *Proc. 12 International Conference on SMFE* (Rio de Janeiro), 679-682.

Andrus, R.D. (1994): In situ characterization of gravelly soils that liquefied in the 1983 Borah Peak Earthquake, *PhD. Dissertation*, University of Texas at Austin, USA.

Andrus, R. D., and Stokoe, H. S. II (2000): Liquefaction resistance of soils from shear-wave velocity, *J. Geotech. & Geoenviron. Eng.*, ASCE, 126, No.11, 1015-1025.

Arai, R. (2014): Effect of Initial Shear Stress on liquefaction failure and shear strain development by Hollow Cylindrical Torsional Shear tests, *Master's Thesis*, Graduate School of Science & Engineering, Chuo University, Japan, in Japanese.

Boulanger, R. W., and Truman, S. P. (1996): Void redistribution in sand under post-earthquake loading. *Canadian Geotech. J.*, Vol 33. 829-833

Casagrande, A. (1971): On liquefaction phenomena, *Geotechnique*, England, XXI, No.3, 197-202.

Castro, G. (1975): Liquefaction and cyclic mobility of saturated sands, *Proc. ASCE*, 101, GT6, 551-569.

Coulter, H. W., and Migliaccio, R. R. (1966) : Effects of the Earthquake of March 27, 1964 at Valdez, Alaska, *Geological Survey Professional Paper* 542-C, U. S. Department of the Interior, USA.

De Alba, P., Seed, H. B. and Chan C. K. (1976): Sand liquefaction in large-scale simple shear tests, *J. Geotechnical Eng.,* ASCE, 102, GT9, 909-927.

Elgamal, A. W., Dobry, R. and Adalier, K. (1989): Study of effect of clay layers on liquefaction of sand deposits using small scale models, *Proc. 2nd US-Japan Workshop on Liquefaction, Large Ground Deformation and Their Effects on Lifelines*, NCEER, SUNY-Buffalo, 233-245.

Field, M. E., Gardner, J. V., Jennings, A. E. and Edwards, B. D. (1982): Earthquake-induced sediment failures on a 0.25° slope, Klamath River delta, California, *Geology* 10, 542-546.

Finn, W.D.L, (1982): Soil liquefaction studies in the People's Republic of China, *Soil Mechanics-Transient and Cyclic Loads*, John Wiley & Sons, Ltd., Ch.22, 609-626.

Hamada, M. (1992): Large ground deformations and their effects on lifelines: 1964 Niigata earthquake. *Case Studies of Liquefaction and Lifeline Performance during Past Earthquakes*, *Vol.1, Japanese Case Studies*, pp. 3.1 - 3.123.

Hiraoka, R. (2000): The effect of physical properties on liquefiability of gravelly soils, *Master's Thesis*, Graduate School of Science & Engineering, Chuo University, Japan, in Japanese.

Idriss, I.M. and Boulanger, R. (2008): Soil liquefaction during earthquakes, *Earthquake Engineering Research Institute*, MNO-12, 29.

Inagaki, H., Iai, S., Sugano, T., Yamazaki, H. and Inatomi, T. (1996): Performance of caisson type quay walls at Kobe Port, Special Issue, *Soils and Foundations*, Japanese Geotechnical Society, 119-136.

Ishihara, K., Tatsuoka, F. and Yasuda, S. (1975): Undrained deformation and liquefaction of sand under cyclic stresses, *Soils and Foundations*, Japanese Geotechnical Society, 15, No.1, 29-44.

Ishihara, K., Iwamoto, S., Yasuda, S. and Takatsu, H. (1977): Liquefaction of anisotropically consolidated sand, *Proc. 9th ICSMGE,* Tokyo, Vol.2, 261-264.

Ishihara, K. and Takatsu, H. (1979): Effects of overconsolidation and K0 conditions on the liquefaction characteristics of sands, *Soils and Foundations*, Japanese Geotechnical Society, 19, No.4, 59-68.

Ishihara, K., Kokusho, T. and Silver, M. (1992): State of the art report: Recent developments in evaluating liquefaction characteristics of local soils, *Proc. 12 International Conference on SMFE* (Rio de Janeiro), 2719-2732.

Ishihara, K. (1993): Liquefaction and flow failure during earthquakes, *Geotechnique*, England, 43, No.3, 351-415.

Japan Road Association (2012): Specifications for highway bridges, *Earthquake Design Manual*, in Japanese.

Kamikawa, T. (2004): Mechanism for water film generation by model tests in 1-dimensional soil container, *Master's Thesis*, Graduate School of Science & Engineering, Chuo University, Japan, in Japanese.

Kokusho, T. Yoshida, Y. Nishi, K. and Esashi, Y. (1983): Evaluation of seismic stability of dense sand layer (Part 1) -Dynamic strength characteristics of dense sand-, *Research Report* No.383025, Central Research Institute of Electric Power Industry, Japan, in Japanese.

Kokusho,T. Yoshida, Y. and Nagasaki, K (1985): Liquefaction strength evaluation of dense sand layer, *Proc. 11th Intern. Conf. on SMFE* (San Francisco), 4, 1897-1900

Kokusho,T., Tanaka,Y., Kawai, T., Kudo, K., Suzuki, K., Tohda, S. and Abe, S. (1995): Case study of rock debris avalanche gravel liquefied during 1993 Hokkaido-Nansei-Oki Earthquake, *Soils and Foundations*, Japanese Geotechnical Society, 35, No.3, 83-95

Kokusho, T. and Yoshida, Y (1997): SPT N-value and S-wave velocity for gravelly soils with different grain size distribution, *Soils & Foundations*, Japanese Geotechnical Society, 37, No.4, 105-113.

Kokusho, T. (1999): Formation of water film in liquefied sand and its effect on lateral spread, *J. Geotech. & Geoenviron. Eng.*, ASCE, 125, No.10, 817-826.

Kokusho, T. and Kojima, T. (2002): Mechanism for post-liquefaction water film generation in layered sand, *J. Geotech. & Geoenviron. Eng.*, ASCE, 128, No.2, 129-137.

Kokusho, T. (2003): Current state of research on flow failure considering void redistribution in liquefied deposits, *Soil Dynamics and Earthquake Engineering*, Elsevier, 23 , 585-603.

Kokusho, T. and Fujita, K. (2002): Site investigation for involvement of water films in lateral flow in liquefied ground, *J. Geotech. & Geoenviron. Eng.*, ASCE, 125, No.10, 817-826.

Kokusho, T., Hara, T. and Hiraoka, R. (2004): Undrained shear strength of granular soils with different particle gradations, *J. Geotech. & Geoenviron. Eng.*, ASCE, 130, No.6, 621-629.

Kokusho, T. (2006): Recent developments in liquefaction research learned from earthquake damage, *Journal of Disaster Research*, Fuji Technology Press, Japan, 1, No.2, 226-243.

Kokusho, T. (2007): Liquefaction strengths of poorly-graded and well-graded granular soils investigated by lab tests, *Proc. 4th International Conference on Earthquake Geotechnical Engineering* (Thessaloniki), Springer, 159-184.

Kokusho, T., Ito, F., Nagao, Y. and Green, R. (2012): Influence of non/low-plastic fines and associated aging effects on liquefaction resistance, *J. Geotech. & Geoenviron. Eng.*, ASCE, 138, No.6, 747-756.

Kokusho, T., Mukai, A. and Kojima, T. (2014): Liquefaction behavior in Urayasu and physical properties of fines, *Proc. 14th Japan Earthquake Engineering Symposium*, Japanese Association of Earthquake Engineering, G06, Thu-2, in Japanese.

Koseki, K. lshihara, K. and Fujii, M. (1986): Cyclic triaxia1tests of sand containing fines, *Proc. 21st Annual Conference of Japanese Geotechnical Society*, JGS, 595-596, in Japanese.

Kulasingam, R., Malvick, E.J., Boulanger, R.W., and Kutter, B.L. (2004): Strength loss and localization of silt interlayers in slopes of liquefied sand, *J. Geotech. & Geoenvir on. Eng.*, ASCE, 130, No. 11, 1192-1202.

Kusaka, T. (2013): Liquefaction of fines-containing sands under initial shear stress by cyclic and monotonic loading torsional shear tests, *Master's Thesis*, Graduate School of Science & Engineering, Chuo University, Japan, in Japanese.

Malvick, E. J., (2005): Void redistribution-induced shear localization and deformation in slope. *Ph.D. Thesis*, University of California, Davis, USA.

Matsuo, O. (1997): Liquefaction potential evaluation methods and earthquake design, *Kiso-ko*, So-go Doboku Kenkyu-jo Co., No. 3, 1997, 34-39, in Japanese.

Matsuo, O. Murata, K. (1997): A proposal of simplified evaluation methods of liquefaction resistance on gravelly soils, *Proc. 32nd Annual Conference of Japanese Geotechnical Society*, JGS, 775-776, in Japanese.

Maurer: B.W., Green, R.A., and Taylor, O.S. (2015): Moving towards an improved index for assessing liquefaction hazard, lessons from historical data, *Soils and Foundations*, Japanese Geotechnical Society, 55 No. 4, in print.

Mori, S. Numata, A., Sakaino, N. and Hasegawa, M. (1991): Characteristics of liquefied sands on reclaimed lands during earthquakes, Tsuchi-to-kiso, Japanese Geotechnical Society, 39, No. 2, 17-22, in Japanese.

Mulilis, J. P., Seed, H. B., Chan, C. K., Michell, J. K. and Arulanandan, K. (1977): Effect of sample preparation on sand liquefaction, *J. Geotech. & Geoenvir on. Eng.*, ASCE, 103 GT2, 91-108.

NRC: National Research Council (1985): Liquefaction of soils during earthquakes, *Committee Report of Earthquake Engineering*, Commission of Engineering and Technical Systems, National Academy Press, Washington, D.C. USA.

Naesgaard, E., and Byrne, P. M., (2005): Flow liquefaction due to mixing of layered deposits, *Proc. of Geot. Earthquake Eng. Satellite Conf., TC4 Committee*, ISSMGE, Osaka, Japan.

Naesgaard, E. (2011): A hybrid effective stress – total stress procedure for analyzing soil embankments subjected to potential liquefaction and flow, *PhD Thesis*, The Faculty of Graduate Studies, The University of British Columbia, Canada.

Olson, S. M. and Stark, T. M. (2002): Liquefied strength ratio from liquefaction flow failure case histories, *Canadian*

Geotechnical Journal, No.39, 629-647.
Papadopoulou, A. and Tika, T. (2008), The effect of fines on critical state and liquefaction resistance characteristics of non-plastic silty sands, *Soils & Foundations*, Japanese Geotechnical Society, 48, No.5, 713-725.
Sasaoka, R. and Kokusho, T. (2015): Liquefaction Resistance versus S-wave Velocity Relationship for Intact and Reconstituted Sands by Bender Element Triaxial Tests, Proc. 6th International Conference on Earthquake Geotechnical Engineering, Christchurch, in print.
Scott, R. F. and Zuckerman K. A. (1972): Sand blows and liquefaction. Proc. *The Great Alaska Earthquake of 1964*- Engineering Publication 1606; National Academy of Sciences, Washington, D.C., 179-189.
Seed H.B. and Lee, K.L. (1966): Liquefaction of saturated sands during cyclic loading, *Proc. ASCE*, SM6, 105-134.
Seed, H. B. and Peacock, W. H. (1971): Test procedures for measuring soil liquefaction characteristics, *Proc. ASCE*, SM8, 1099-1119.
Seed, H. B., Mori, K. and Chan C. K. (1977): Influence of Seismic history on Liquefaction of sands, *J. Geotech. Eng.*, ASCE, 103, GT4, 257-270.
Seed, H.B. and Idriss, I.M. (1981): Evaluation of liquefaction potential of sand deposits based on observations of performance in previous earthquakes, *Preprint 81-544, In Situ Testing to Evaluate Liquefaction Susceptibility*, ASCE National Convention.
Seed, H. B. and De Alba, P. (1984): Use of SPT and CPT tests for evaluating the liquefaction resistance of sands, *Proc. In-situ'86*, ASCE Geotech. Special Publication, No.6, 281-302.
Seed, H. B., Tokimatsu, K., Harder, L. F. Jr. and Chung, R. (1985): Influence of SPT procedures in soil liquefaction resistance evaluations, *Journal of Geotech. Eng.*, ASCE 111, No.12, 1425-1445.
Seed, H.B. (1987): Design problems in soil liquefaction, *Journal of Geotech. Eng.* ASCE, 113, No.8, pp.827-845.
Suzuki, T. and Toki, S. (1984): Effects of preshearing on liquefaction characteristics of saturated sand subjected to cyclic loading, *Soils and Foundations*, Japanese Geotechnical Society, 24, No.2, 16-28.
Suzuki, Y., Tokimatsu, K., Taya, Y. and Kubota, Y. (1995): Correlation between CPT data and dynamic properties of in situ frozen samples, *Proc. 3rd Intern. Conf. on Recent Advances in Geotech. Earthquake Eng. & Soil Dynamics*, Vol.1, 249-252.
Tanaka, Y., Kudo, K., Yoshida, Y. and Kokusho, T. (1992): Undrained cyclic strength of gravelly soil and its evaluation by penetration resistance and shear modulus, *Soils and Foundations,* Japanese Geotechnical Society, 32 (4), 128-142.
Tatsuoka, F., Iwasaki, T. Tokida, K. and Konno, M. (1981): Cyclic undrained triaxial strength of sampled sand affected by confining pressure, *Soils and Foundations*, Japanese Geotechnical Society, 21, No.2, 115-120.
Tatsuoka, F., Muramatsu, M. and Sasaki, T. (1982): Cyclic undrained stress-strain behavior of dense sands by torsional simple shear test, *Soils and Foundations*, Japanese Geotechnical Society, 22, No.2, 55-70.
Tatsuoka, F., Kato, H., Kimra, M. and Pradhan, T.B.S. (1988): Liquefaction strength of sands subjected to sustained pressure, *Soils and Foundations*, Japanese Geotechnical Society, 28, No.1, 119-131.
Tokimatsu, K. and Yoshimi, Y. (1983): Empirical coorelation of soil liquefaction based on SPT N-value and fines content, *Soils and Foundations*, Japanese Geotechnical Society, 23, No.4, 56-74.
Tokimatsu, K., Yamazaki, T. and Yoshimi, Y. (1986): Soil liquefaction evaluations by elastic shear moduli, *Soils & Foundations*, Japanese Geotechnical Society, Vol.26, No.1, 25-35.
Vaid, Y. P. and Chern J. C. (1983): Effect of static shear on resistance to liquefaction, *Soils and Foundations*, Japanese Geotechnical Society, 23, No.1, 47-60.
Vaid, Y. P. and Chern, J. C. (1985): Cyclic and monotonic undrained response of saturated sands, *Proc. Advances in the art of testing soils under cyclic conditions*, ASCE Covention, Detroit, Mich, 120-147.
Yamashita, S. and Toki, S. (1992): Effects of fabric anisotropy of sand on cyclic undrained triaxial and torsional strengths, *Soils and Foundations*, Japanese Geotechnical Society, 33 No. 3, 92-104.
Yoshimi, Y. and Oh-oka, H. (1975): Influence of degree of shear stress reversal on the liquefaction potential of saturated sand, *Soils and Foundations*, Japanese Geotechnical Society, 15, No.3, 27-40.
Yoshimi, Y., Hatanaka, M. and Oh-oka, H. (1978): Undistutbed sampling of saturated sands by freezing, *Soils and Foundations*, Japanese Geotechnical Society, 18, No.3, 59-73.
Yoshimi, Y. (1991): Particle grading and plasticity of hydraulically filled soils and their liquefaction resistance, *Tsuchi-to-Kiso*, Japanese Geotechnical Society, 39, No.8, 49-50, in Japanese.
Yoshimi, Y., Tokimatsu, K. and Ohara, J. (1994): In situ liquefaction resistance of clean sands over a wide density range, *Geotechnique*, England, 44, No.3, 479-494.
Yoshimi, Y. (1994): Relationship among liquefaction resistance, SPT N-value and relative density for undisturbed samples of sands, *Tsuchi-to-Kiso*, Japanese Geotechnical Society, in Japanese, 42 No.4, 63-67.